

# The *Far Ultraviolet Spectroscopic Explorer* Legacy in the Magellanic Clouds: An Online Stellar Sight Line Atlas<sup>1</sup>

WILLIAM P. BLAIR,<sup>2</sup> CRISTINA OLIVEIRA,<sup>2</sup> STEPHANIE LAMASSA,<sup>2</sup> SERAH GUTMAN,<sup>2</sup> CHARLES W. DANFORTH,<sup>3</sup>  
ALEX W. FULLERTON,<sup>4</sup> RAVI SANKRIT,<sup>5</sup> AND ROBERT GRUENDL<sup>6</sup>

Received 2009 March 6; accepted 2009 May 8; published 2009 May 28

**ABSTRACT.** We present an atlas of stellar sight line data from the Far Ultraviolet Spectroscopic Explorer (*FUSE*) satellite for 287 stars in the Magellanic Clouds, obtained from eight years of satellite operations. The intent of our project is to make this rich ensemble data set accessible to a broad community of researchers in a standardized format that will enable easy identification of subsets of these data that are appropriate for pursuing specific science programs. We present the data in a standardized manner, showing key interstellar lines on a velocity scale, optical (MCELS) and infrared (*Spitzer*) sight line context images, and overview plots of the spectral region containing the O VI  $\lambda\lambda$ 1032, 1038 doublet, and the entire 905–1187 Å spectral range observed with *FUSE*. Objects with multiple observations have had their data summed to directly provide the highest signal-to-noise ratio available. These data are accessible online as a High Level Science Product through the Multimission Archive at Space Telescope (MAST). In this article, we describe the data sets and processing, the atlas materials, and the MAST interface in detail, and also provide examples of how to use these materials.

## 1. INTRODUCTION

Over nearly eight years of operations, the Far Ultraviolet Spectroscopic Explorer (*FUSE*) satellite was used by numerous observers to obtain high resolution ( $R \approx 20,000$ ) far-ultraviolet (905–1187 Å) spectra of nearly 300 stars in the Magellanic Clouds, mostly of spectral types O and B. Each spectrum contains information about the star observed as well as the interstellar material along each sight line, both from the Milky Way disk and halo (near zero velocity) and from within the host galaxy ( $v_{\text{LMC}} \approx 264 \text{ km s}^{-1}$ ;  $v_{\text{SMC}} \approx 165 \text{ km s}^{-1}$ ). Furthermore, the *FUSE* spectral range contains absorption lines from tracers of cold, warm, and hot interstellar gas. The ensemble data set is thus extremely rich in information, with application to a broad range of potential scientific topics. Many important investigations were published with the subset of sight lines that were available during the first few years of *FUSE* operations

(e.g., Massa et al. 2000; Sembach et al. 2001; Hutchings & Giasson 2001; Tumlinson et al. 2002; Hoopes et al. 2002; Howk et al. 2002a, 2002b; Walborn et al. 2002; Massa et al. 2003). However, now that a much more extensive set of observations is available, how does one assess these data and find those observations that are of potential interest to investigating a particular scientific problem?

We have undertaken a project to make the *FUSE* Magellanic Clouds data available to the broader community of researchers in a format that allows both quick-look access and assessment of the various data sets for applicability to a given scientific problem, as well as providing context for the interstellar material potentially along each sight line. In many ways, this work follows on to the first *FUSE* sight line atlas published by Danforth et al. (2002), although we have expanded on that work in several significant ways. We have reprocessed all data with the final *FUSE* calibration pipeline (CalFUSE 3.2) to ensure uniformity. For single observations, these products are the same as available directly from MAST, but we have combined multiple data sets on the same object when appropriate, and produced summary spectra in various formats to provide an overview of the interstellar medium (ISM) and stellar spectral characteristics of each data set. We also provide optical and infrared context images centered on each *FUSE* target. These products are available as a High Level Science Product (HLSP) through an online interface available at the Multimission Archive at Space Telescope (MAST).<sup>7</sup>

---

<sup>1</sup> Based on observations made with the NASA-CNES-CSA Far Ultraviolet Spectroscopic Explorer. *FUSE* was operated for NASA by the Johns Hopkins University under NASA contract NAS 5-32985.

<sup>2</sup> Department of Physics and Astronomy, The Johns Hopkins University, Baltimore, MD 21218; wpb@pha.jhu.edu, oliveira@jhu.edu, steph@pha.jhu.edu, serahg@gmail.com.

<sup>3</sup> Center for Astrophysics and Space Astronomy, University of Colorado, Boulder, CO 80309; danforth@casa.colorado.edu.

<sup>4</sup> Space Telescope Science Institute, Baltimore, MD 21218; fullerton@stsci.edu.

<sup>5</sup> SOFIA, Universities Space Research Association, Moffett Field, CA, 94035; rsankrit@sofia.usra.edu.

<sup>6</sup> Department of Astronomy, University of Illinois, Urbana, IL 61801; gruendl@uiuc.edu.

---

<sup>7</sup> See [http://archive.stsci.edu/prepds/fuse\\_mc](http://archive.stsci.edu/prepds/fuse_mc).

There are many ways the community may choose to use the *FUSE* atlas and supporting materials. A few examples include (a) identifying which sight lines show strong molecular hydrogen absorption at Magellanic velocities, and whether this is correlated with the appearance of those sight lines on the IR context images or with  $E(B - V)$  value; (b) finding those stellar sources whose continuum allows interstellar O VI lines to be measured, to study the hot gas distribution; (c) identifying pairs or groups of sight lines that provide potential comparisons (say within bright nebulae and adjacent), for studying nebular structures; (d) identifying sight lines with particularly high (or low) values of Fe II/Fe III to study ionization effects, (e) finding the best pairings of stars by spectral type and  $E(B - V)$  to study the far-UV extinction curve in the LMC versus the SMC, or (f) identifying the appropriate subset of LMC or SMC O stars that show obvious P Cygni wind profiles for further analysis. Each of these projects requires sifting through numerous potential spectra to find the relevant data prior to performing the detailed analysis.

In this article, we describe the online resource we have created, including the data processing, the context images provided for each sight line, and the MAST HLSP interface. We conclude with examples to illustrate how these products might be used.

## 2. OBJECT SAMPLE AND FUSE DATA PROCESSING

### 2.1. FUSE Overview

Background information and descriptions of on-orbit performance of the *FUSE* satellite are provided by Moos et al. (2000) and Sahnou et al. (2000), with updates in Moos et al. (2002). Significant information is also available through the *FUSE* archival web site, which is also hosted at MAST.<sup>8</sup> Briefly, the *FUSE* instrument covers the wavelength range 905–1187 Å, with a nominal point source resolution  $R = \lambda/\Delta\lambda \approx 20,000$ . *FUSE* contains four optical paths, or channels, each with its own primary mirror, focal plane and spectrograph aperture plate, and grating. The channels are referred to as LiF1, LiF2, SiC1, and SiC2, where LiF and SiC refer to the optical coatings on each channel and the numbers refer to one of two microchannel plate detectors. Furthermore, each detector is subdivided into two segments, A and B, whose boundaries in wavelength space are offset slightly so that full wavelength coverage is maintained. See § 3 of Moos et al. (2000) for full details.

The aperture plate for each channel contained three observing apertures, referred to as LWRS (30" square), MDRS (4" × 20"), and HIRS (1.25" × 20"). Small, thermally-induced distortions in the *FUSE* optical bench discovered after launch did not allow rigid coalignment of the apertures from each

channel over time. Typical misalignments varied from a few to as much as 10", and could vary even during the course of a given orbit or integration. Observations obtained using the LWRS aperture typically have solid data in all channels, but observations using the smaller MDRS or HIRS apertures may have lower-than-expected signal level in channels other than the guide channel due to these thermal motions.<sup>9</sup> On the other hand, the use of the LWRS aperture in the relatively crowded fields in the Magellanic Clouds sometimes resulted in multiple stars being present, thus compromising the data quality. In these cases, data from MDRS or HIRS observations that excluded other contaminating stars would be preferable. For stars observed in LWRS, the data processing effectively removed the thermal motions, leaving no discernible impact on the data quality or resolution.

### 2.2. Object Selection and Information

We have selected all *FUSE* observations within designated R.A. and decl. ranges as being potential LMC and SMC observations. We used  $\alpha(\text{J2000}) = 4^{\text{h}}40^{\text{m}}$  to  $6^{\text{h}}00^{\text{m}}$ ,  $\delta(\text{J2000}) = -65^\circ$  to  $-72^\circ$  for the LMC, and  $\alpha(\text{J2000}) = 0^{\text{h}}40^{\text{m}}$  to  $1^{\text{h}}40^{\text{m}}$ ,  $\delta(\text{J2000}) = -71^\circ$  to  $-74^\circ$  for the SMC. We then subset this list by using the user-defined *FUSE* "Spectral Type" designation to select only observations whose primary target was a stellar source type. This produced lists that included 187 unique objects in the LMC and 100 objects in the SMC, totaling ~500 separate *FUSE* observations. The global spatial distribution of these sight lines is shown on color images constructed from Magellanic Cloud Emission Line Survey data (MCELS; see Smith et al. 1999, 2004) of the LMC in Figure 1 and the SMC in Figure 2. The figure captions describe the symbols used. Tables 1 and 2 provide the master lists of objects in each galaxy that are included in the *FUSE* Magellanic Cloud Legacy project, and are identical in content and nearly identical in format to the online versions<sup>10</sup>.

The FITS file headers for each data set contain photometric and spectral type information that was provided by the original observers. However, the sources for this information were not provided. To provide more uniform and self-consistent data in the atlas, we have performed extensive literature searches to improve the listed spectral types and photometric information provided in the *FUSE* Tables and encoded references for the information used. The identifications for the references are given at the bottom of Tables 1 and 2. If no better information was located in the literature, the reference "FH" refers to the FITS header information.

<sup>9</sup>The SIMBAD database is operated at CDS, Strasbourg, France, and is available at <http://simbad.u-strasbg.fr/simbad/>.

<sup>10</sup>See <http://ssc.spitzer.caltech.edu/ost>.

<sup>8</sup>See <http://archive.stsci.edu/fuse/>.

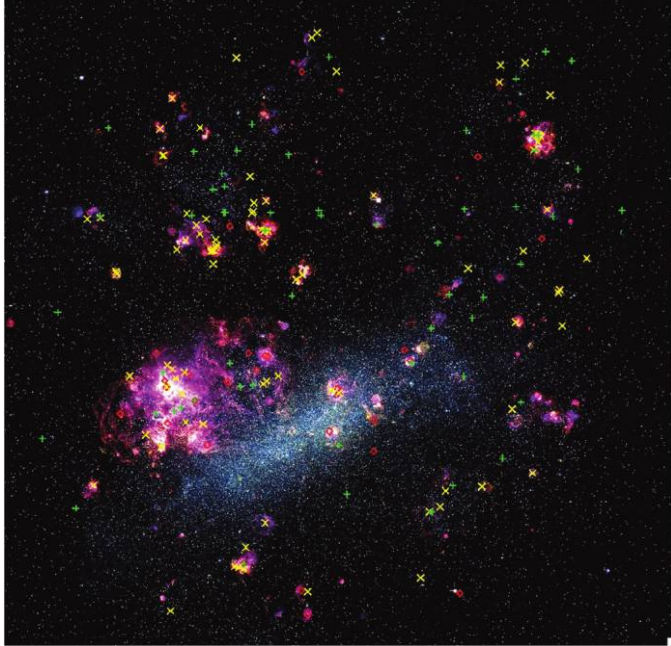


FIG. 1.—Overview image of the Large Magellanic Cloud showing the global distribution of *FUSE* stellar observations. The underlying image is a three-color image made from MCELS data, with  $H\alpha$  in *red*,  $[S\ II]$  in *green*, and  $[O\ III]$  in *blue*, all without star subtraction. Three different symbols are shown, indicating objects with spectral types of O (*blue X symbols*), B (*green plus symbols*), and other (WR stars, LBV, etc.; *red diamonds*).

### 2.3. *FUSE* Data Processing

Each *FUSE* observation-level data set has been reprocessed with version 3.2 of the CalFUSE pipeline. This is significant

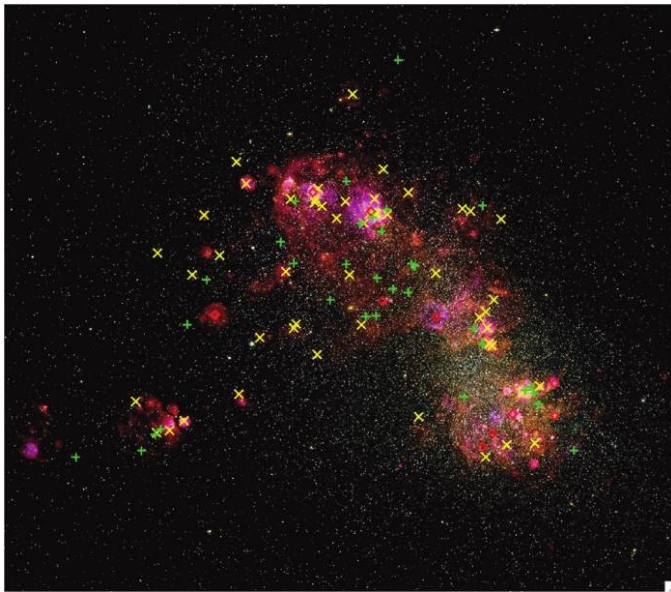


FIG. 2.—Same as Figure 1, but for the SMC.

even for previously published data sets because CalFUSE 3 and higher versions were updated extensively from earlier versions of the pipeline processing, as described in detail by Dixon et al. (2007). CalFUSE 3.2 is the archival version of the *FUSE* calibration pipeline, updated at the end of *FUSE* operations and including all significant improvements to flux calibration and pointing corrections. Thus, the Legacy project data sets are as good as can be produced by an automated pipeline, which satisfies our goal of providing the best data possible for generalized quick-look assessment purposes.

CalFUSE 3.2 produces fully calibrated data sets for each observation and channel, summing all exposures of a given observation. CalFUSE 3.2 also produces a summary file called the NVO file<sup>11</sup>, where the software inspects the data in each channel and constructs the best available summary data set over the entire *FUSE* wavelength range. We have found it satisfactory to use the NVO files directly for all objects where a single *FUSE* observation was obtained. We note, however, that any automated processing system includes some simplifying assumptions. Users may find it beneficial to reprocess individual *FUSE* data sets to their own specifications for detailed scientific analysis.

For each MC object with multiple observations in a given aperture, all observations were aligned and co-added to produce the highest signal-to-noise ratio (S/N) single data set available. If data were obtained through multiple apertures, the smaller aperture data were chosen in order to decrease contamination by airglow and (potentially) from nearby stars, unless the smaller aperture data were clearly of inferior quality or lower S/N. Objects with combined data are indicated by “Number of Data Sets” values greater than 1 in Tables 1 and 2. If objects were observed several times under different program IDs, the summed FITS files contain that information as comments in the header section. The summed files are named using the *FUSE* ID corresponding to the observation with the longest exposure time. The total exposure time contained in the header and in the Tables is the sum of the exposure times for the separate data sets that were combined.

To co-add multiple observations, we used the *\*all\*.fits* files (four files per observation) produced by the CalFUSE pipeline (see Dixon et al. 2007). The individual observation *\*all\*.fits* files were aligned to each other using an IDL cross-correlation routine and then combined, using the exposure time for weighting. We also co-added the *\*nvo\*.fits* files produced by CalFUSE, which were used only to produce the highly binned plot that covers the whole *FUSE* spectral region (described in § 3.2). The combined data files are available for download directly from the MAST/*FUSE* MC Legacy website, providing added value to those desiring the highest available quality in S/N data sets (e.g., for ISM work). Those more interested in

<sup>11</sup>For reference, the LiF1 channel was used for guiding from launch until 2005 July 12, and the LiF2 channel was used after that date.

TABLE 1  
FUSE LMC OBJECTS AND INFORMATION

FUSEID <sup>a</sup>	Object Name <sup>b</sup>	R.A. (J2000)	Decl. (J2000)	Sp. Type	Sp. Type Ref. <sup>d</sup>	V	(B - V)	Photo Ref. <sup>d</sup>	E(B - V)	Aperture <sup>c</sup>	Num DS <sup>e</sup>	Exp. Time <sup>b</sup> (ks)
B08601	SK-67 2	04 47 04.4	-67 06 53.1	B1Ia+	F91	11.07	-	FH	0.26	LWRS	1	6.6
P10307	SK-67 05	04 50 18.9	-67 39 37.9	O9.7Ib	W77	11.34	-0.12	A72	0.15	LWRS	2	7.4
A04904	SK-68 03	04 52 15.5	-68 24 26.9	O9I	C86	13.13	-0.13	I79	0.48	LWRS	2	9.2
C16006	SK-66 01	04 52 18.9	-66 43 52.8	B1.5Ia	F88	11.61	-	FH	0.10	LWRS	1	8.9
E51118	B1I2	04 53 00.8	-68 01 32.5	O7.5III	M02	13.50	-0.20	M02	0.10	LWRS	1	11.8
E51119	B1I3	04 53 06.4	-68 03 23.1	O6.5V	M02	13.75	-0.09	M02	0.21	LWRS	1	23.5
D09810	SK-70 13	04 54 01.1	-69 59 47.4	O9V	M02	12.29	-0.14	M02	0.18	MDRS	1	7.9
A04903	SK-65 01	04 54 06.6	-65 35 22.5	B0.5I	J01	12.50	-	FH	0.15	LWRS	1	6.2
P11742	SK-67 14	04 54 31.9	-67 15 24.9	B1.5Ia	F88	11.52	-0.10	A72	0.10	LWRS	3	14.4
D09808	SK-67 18	04 55 14.9	-67 11 24.5	O6-7n-nm+WN5-6A	W77	11.95	-	FH	0.10	MDRS	1	7.9
P11744	HD32109	04 55 31.5	-67 30 01.0	WN4b	S96	13.86	-0.28	F83	0.00	LWRS	2	16.1
A04901	SK-66 18	04 55 59.8	-65 58 30.0	O6V(f)	M95	13.50	-0.20	I79	0.12	LWRS	1	3.2
B12806	HD268809	04 56 10.5	-69 15 38.4	B0.5Ia	F88	11.94	-	FH	0.11	LWRS	1	5.7
B01010	PGMW-1210	04 56 34.7	-66 28 25.7	blend	FH	12.61	-0.31	P92	0.02	MDRS	1	5.9
B01001	PGMW-3053	04 56 41.0	-66 24 40.2	O5.5I-III	FH	13.13	-0.09	P92	0.24	MDRS	1	8.4
B01002	PGMW-3070	04 56 43.2	-66 25 02.0	O6V	FH	12.75	-0.22	P92	0.11	MDRS	1	6.4
D03002	LH103073	04 56 43.3	-66 24 54.1	O6.5Vz	FH	14.71	-0.10	P92	0.22	MDRS	1	24.3
D03003	LH103102	04 56 45.4	-66 24 45.9	O7Vz	FH	13.55	-0.10	P92	0.22	MDRS	1	15.7
B01003	PGMW-3120	04 56 46.8	-66 24 46.6	O5.5V	FH	12.80	-0.07	P92	0.26	MDRS	1	7.4
B01004	PGMW-3157	04 56 50.5	-66 24 35.0	BC1Ia	FH	12.47	-0.02	P92	0.19	MDRS	1	8.3
Z91213	SK-65 2	04 56 51.5	-65 31 08.3	B1V	M95	12.83	-	FH	0.11	LWRS	1	12.8
B01005	PGMW-3168	04 56 54.4	-66 24 15.9	O7II	FH	13.68	-0.11	P92	0.22	MDRS	1	10.7
D03001	LH91486	04 56 55.5	-66 28 58.0	O6.5Vz	FH	14.20	-0.21	P92	0.11	MDRS	1	9.0
D03004	LH103204	04 56 58.7	-66 24 40.5	O6-7Vz	FH	14.02	-0.17	P92	0.15	MDRS	1	12.8
B01006	PGMW-3209	04 56 58.9	-66 24 38.0	O3III	FH	12.66	-0.11	P92	0.22	MDRS	1	4.5
B01007	PGMW-3223	04 57 00.8	-66 24 25.2	O8.5IV	FH	12.95	-0.12	P92	0.21	MDRS	1	7.1
B08603	SK-66 35	04 57 04.5	-66 34 38.4	BC1Ia	F91	11.58	-0.08	F88	0.11	MDRS	1	4.5
E51120	SK-69 50	04 57 15.1	-69 20 20.4	O7If	M02	13.31	-0.16	M02	0.14	LWRS	1	9.3
F92706	HV2241	04 57 15.7	-66 33 54.5	O7III	FH	13.50	-	FH	0.20	LWRS	5	67.0
B01008	PGMW-3264	04 57 16.2	-66 23 21.2	O3-O6V	FH	14.21	-0.33	P92	0.01	MDRS	1	4.6
B01009	PGMW-3271	04 57 21.9	-66 24 27.1	BIII	FH	12.99	-0.13	P92	0.08	MDRS	1	4.5
E51121	SK-68 15	04 57 24.1	-68 23 57.5	WC4	M02	12.90	-0.13	M02	0.24	MDRS	1	11.1
C00204	SK-67 22	04 57 27.5	-67 39 03.0	O3If*/WN6	M02	13.44	-0.18	W82	0.16	LWRS	1	4.9
C14005	SK-67 23	04 57 37.0	-67 47 38.0	BE	M02	12.47	+0.07	M02	0.20	LWRS	1	17.8
E51122	SK-68 16	04 57 37.8	-68 24 36.1	O7III	M02	12.85	-0.19	M02	0.24	MDRS	1	8.5
C14003	SK-66 40	04 57 44.2	-66 32 54.7	WN10h	FH	13.00	-	FH	0.25	MDRS	1	3.1
P11743	SK-69 52	04 57 48.5	-69 52 22.0	B2Ia	F88	11.50	-0.03	A72	0.17	LWRS	1	5.5
A04902	SK-67 28	04 58 39.2	-67 11 18.9	B0.7Ia	F88	12.28	-0.14	I82	0.10	LWRS	2	11.8
E51123	SK-65 05	04 58 52.7	-65 39 05.3	O9II	FH	12.65	-	FH	0.17	LWRS	1	2.7
B08610	SK-65 15	04 59 41.4	-65 49 50.1	B1Ia	F88	11.77	-	FH	0.12	MDRS	1	4.3
E51124	SK-67 32	04 59 51.6	-67 56 55.9	WN4b	M02	14.48	-0.21	M02	0.09	LWRS	1	28.8

TABLE 1 (Continued)

<i>FUSEID</i> <sup>a</sup>	Object Name <sup>a</sup>	R.A. (J2000)	Decl. (J2000)	Sp. Type	Sp. Type Ref. <sup>d</sup>	<i>V</i>	( <i>B</i> - <i>V</i> )	Photo Ref. <sup>d</sup>	<i>E</i> ( <i>B</i> - <i>V</i> )	Aperture <sup>c</sup>	Num DS <sup>a</sup>	Exp. Time <sup>a</sup> (ks)
E51125	SK-70 32	05 00 10.3	-70 11 09.7	O9.5II	M02	13.06	-0.21	M02	0.09	MDRS	1	10.7
P10309	SK-65 21	05 01 22.3	-65 41 48.1	O9.7Iab	W95	12.02	-0.16	175	0.20	LWRS	4	17.5
P10310	SK-65 22	05 01 23.1	-65 52 33.5	O6Iaf+	W77	12.07	-0.19	179	0.20	LWRS	1	27.2
B08602	SK-68 26	05 01 32.2	-68 10 43.1	BC2Ia	F91	11.54	-	FH	0.31	LWRS	1	11.4
G92702	HD269006	05 02 07.4	-71 20 13.0	LBV	FH	10.70	-	FH	0.00	LWRS	2	18.0
B07702	HV2274	05 02 40.9	-68 24 21.3	B1.5III	FH	14.20	-	FH	0.12	LWRS	1	22.1
P11745	HD33133	05 03 10.2	-66 40 54.0	WN8h	S96	12.71	-0.23	F83	0.08	LWRS	1	4.6
P10311	SK-69 59	05 03 12.7	-69 01 37.2	B0	R78	12.13	-0.12	175	0.20	LWRS	1	25.7
E51126	SK-67 38	05 03 29.7	-67 52 25.5	O8III	M02	13.66	-0.22	M02	0.08	LWRS	1	18.6
C16008	SK-70 50	05 03 45.9	-70 11 57.7	B3Ia	F88	11.20	-	FH	0.10	LWRS	1	12.0
P21501	HD268939	05 04 14.9	-67 15 05.4	B1	FH	10.90	-	FH	0.35	LWRS	1	19.8
D13802	NGC1818-D1	05 04 32.5	-66 24 51.0	B1V	FH	14.93	-	FH	0.09	LWRS	1	28.9
P11720	SK-70 60	05 04 40.9	-70 15 34.5	O4-5V:n	Wpc	13.85	-0.19	R78	0.13	LWRS	1	7.9
P11721	SK-70 69	05 05 18.7	-70 25 49.8	O5V	W95	13.94	-0.27	R78	0.01	LWRS	1	6.1
P11741	SK-68 41	05 05 27.2	-68 10 02.7	B0.5Ia	F88	12.01	-0.14	182	0.16	LWRS	2	11.9
B12808	HD269074	05 06 16.1	-70 29 35.7	B0.7Ia	F88	11.29	-	FH	0.08	LWRS	1	6.2
B09003	SK-70 79	05 06 37.3	-70 29 24.7	B0III	M02	12.71	-0.06	M02	0.27	LWRS	1	19.6
A04915	SK-67 46	05 07 01.6	-67 37 29.6	B1.5I	J01	12.34	-0.06	175	0.14	MDRS	1	3.5
P11740	SK-68 52	05 07 20.6	-68 32 09.6	B0Ia	W77	11.54	-0.07	A72	0.15	LWRS	2	13.1
A04914	SK-71 08	05 07 23.4	-71 11 54.5	O9II	FH	13.25	-	FH	0.08	LWRS	2	10.8
C10303	MACHO79-4779	05 09 29.1	-68 55 03.0	B0V	FH	14.60	-	FH	0.11	LWRS	1	16.6
E51127	SK-68 57	05 09 40.5	-68 53 25.1	WN4b+OB?	M02	13.69	-0.15	M02	0.15	LWRS	1	13.8
C14006	HD-269128	05 10 23.1	-68 46 24.4	LBV(B2.5Iab)	FH	10.40	-	FH	0.24	LWRS	1	6.0
D00601	0513-69	05 13 50.8	-69 51 46.9	CV	FH	16.70	-	FH	0.00	LWRS	8	92.1
E95704	HD34664	05 13 53.1	-67 26 54.4	B0-B0.5	FH	11.52	-	FH	0.00	LWRS	1	24.4
B09004	SK-6979	05 13 54.0	-69 31 48.0	Olatpe	W77	12.00	-	FH	0.30	LWRS	1	7.6
P11717	SK-67 69	05 14 20.1	-67 08 03.5	O4III(f)	G87a	13.09	-0.16	179	0.16	LWRS	1	7.8
A04913	SK-70 85	05 17 05.7	-70 19 23.1	B0	M02	12.32	-0.03	M02	0.15	LWRS	2	15.7
C10301	MACHO78-6097	05 18 04.7	-69 48 19.0	B0V	FH	14.40	-	FH	0.12	LWRS	1	8.3
E51129	B1130	05 18 06.0	-69 14 34.5	O8.5V(f)	M02	12.53	-0.16	M02	0.14	LWRS	1	11.3
Z90502	SK-69 94	05 18 14.5	-69 15 01.0	A0e/LBV	FH	9.72	-	FH	0.10	LWRS	1	8.6
B09005	SK-6995	05 18 19.2	-69 11 40.6	B1Ia+WN3-4	W77	11.31	-	FH	0.20	LWRS	1	8.1
P21702	B1128	05 18 19.9	-65 49 14.0	O9V	M95	13.82	-	FH	0.06	LWRS	1	6.9
P11724	SK-69 104	05 18 59.5	-69 12 54.7	O6Ib(f)	W02b	12.10	-0.21	A72	0.11	LWRS	1	3.9
A04906	SK-65 41	05 19 05.4	-65 40 03.5	B2III	J01	12.82	-	FH	0.11	LWRS	1	3.8
D08801	Brey22	05 19 16.4	-69 39 19.5	O9.5Ib	W77	12.30	-	FH	0.13	MDRS	14	58.1
P10312	SK-67 76	05 20 05.8	-67 21 08.9	B0	R78	12.42	-0.13	175	0.20	LWRS	1	24.7
P11733	SK-65 44	05 20 18.0	-65 24 13.0	O9V	FH	13.65	-	FH	0.10	LWRS	2	9.9
C16009	SK-67 78	05 20 19.1	-67 18 06.1	B3Ia	F88	11.26	-	FH	0.10	LWRS	1	10.2
C00207	SK-6547	05 20 54.7	-65 27 18.1	O4If*	FH	12.57	-	FH	0.12	LWRS	1	7.9
G92705	Brey24	05 21 57.6	-65 48 59.0	WN6	FH	13.30	-	FH	0.08	LWRS	1	30.0
P23201	N44C-Star2	05 22 14.2	-67 58 36.6	O7V	FH	14.20	-	FH	0.00	LWRS	1	19.0
E51130	SK-71 19	05 22 15.8	-71 21 39.9	O6III	FH	14.20	-	FH	0.10	LWRS	1	22.1

TABLE 1 (Continued)

FUSEID <sup>a</sup>	Object Name <sup>a</sup>	R.A. (J2000)	Decl. (J2000)	Sp. Type	Sp. Type Ref. <sup>c</sup>	V	(B - V)	Photo Ref. <sup>d</sup>	E(B - V)	Aperture <sup>e</sup>	Num DS <sup>f</sup>	Exp. Time <sup>g</sup> (ks)
G92706	..... Brey26	05 22 22.5	-71 35 58.0	WN6	FH	12.70	-	FH	0.00	LWRS	1	4.2
B02701	..... HD269445	05 22 59.8	-68 01 46.6	OBf:pe	W77	11.45	-	FH	0.27	LWRS	1	24.7
E51131	..... SK-71 26	05 23 10.0	-71 20 50.7	WC	FH	12.79	-	FH	0.08	LWRS	2	6.1
A04905	..... SK-68 75	05 23 28.5	-68 12 22.8	B1I	J01	12.03	-0.06	A72	0.19	MDRS	2	6.4
B12803	..... SK-66 78	05 23 30.4	-66 42 11.5	B1.5I	J01	12.22	-	FH	0.11	LWRS	1	7.9
P11736	..... SK-69 124	05 25 18.3	-69 03 11.1	O9Ib	C86	12.81	-0.18	I82	0.12	LWRS	2	12.6
B12804	..... HD269504	05 25 38.9	-67 19 00.1	B1Ia	F88	11.95	-	FH	0.08	LWRS	1	5.7
P11734	..... SK-67 101	05 25 56.3	-67 30 28.7	O8II(f)	W02b	12.63	-0.17	I75	0.14	LWRS	3	11.9
P10313	..... SK-67 104	05 26 04.1	-67 29 56.5	WC4(O?)+O8I:	M90	11.44	-0.17	F83	0.20	LWRS	1	5.1
D15301	..... SK-67 105	05 26 06.3	-67 10 57.6	O4f	FH	12.42	-	FH	0.07	LWRS	6	28.4
A11101	..... SK-67 106	05 26 15.2	-67 29 58.3	B0:	R78	11.78	-0.17	R78	0.15	MDRS	1	11.3
A11102	..... SK-67 107	05 26 20.6	-67 29 55.4	B0	R78	12.50	-0.12	I75	0.12	MDRS	1	11.2
F32102	..... LH54-425	05 26 24.2	-67 30 17.2	O3III+O5	FH	13.08	-	FH	0.00	LWRS	4	69.4
E51133	..... SK-67 108	05 26 26.6	-67 37 20.3	O4-5III	M02	12.57	-0.20	M02	0.05	LWRS	1	3.8
C15101	..... HD36521	05 26 30.3	-68 50 25.4	WC4+O6V-III	M90	12.42	-0.23	F83	0.09	LWRS	11	85.8
P20301	..... SK-68 82	05 56 45.3	-68 49 52.8	Wolf-Rayet	FH	09.86	-	FH	0.20	LWRS	4	9.6
P11737	..... B1170	05 26 47.7	-69 06 11.7	O9.5Ib	W02b	13.09	-0.17	B75	0.13	LWRS	1	4.3
C15502	..... SK-67 111	05 26 47.9	-67 29 29.9	O6:iafpe	W02b	12.57	-0.20	I75	0.12	LWRS	19	160.5
P11732	..... B1173	05 27 10.0	-69 07 56.2	O8I:	W02b	13.00	-0.14	B75	0.17	LWRS	2	11.3
E95701	..... SK-66 97	05 27 18.4	-66 22 07.4	B1[e]lab	FH	12.54	-	FH	0.07	LWRS	1	5.8
F92707	..... HV25-43	05 27 27.4	-67 11 55.4	O8+O9	FH	12.92	-	FH	0.12	LWRS	1	5.6
E51134	..... SK-67 118	05 27 33.4	-67 17 30.2	O7V	M02	12.98	-0.19	M02	0.11	LWRS	1	2.8
P11725	..... SK-70 91	05 27 33.7	-70 36 48.3	O2III(dE)+OB	W02b	12.78	-0.23	I79	0.09	LWRS	1	5.5
E51135	..... SK-67 119	05 27 40.7	-67 18 10.6	O7III(f)	M02	13.31	-0.20	M02	0.10	LWRS	1	4.0
P11723	..... SK-66 100	05 27 45.5	-66 55 15.0	O6II(f)	W95	13.26	-0.21	I79	0.12	LWRS	1	7.1
P11747	..... HDE269582	05 27 52.7	-68 59 08.6	WN10h	C97	11.88	-0.04	I75	0.09	LWRS	1	4.6
E95703	..... HDE269599	05 28 22.6	-69 08 32.2	B	FH	10.18	-	FH	0.00	LWRS	1	2.8
B08611	..... SK-65 63	05 28 39.6	-65 39 00.5	O9.7I:	F88	12.56	-	FH	0.15	MDRS	1	4.1
F08901	..... LH64-16	05 28 47.0	-68 47 47.7	O2-O3.5III(f)	W02a	13.62	-0.17	W02a	-	-	2	9.5
B12809	..... SK-66 106	05 29 01.0	-66 38 28.0	B2Ia	F88	12.72	-	FH	0.09	LWRS	1	6.6
C10302	..... HV982	05 29 52.5	-69 09 22.0	B1V	FH	14.60	-	FH	0.09	LWRS	1	14.0
E51136	..... SK-70 97	05 30 11.3	-70 51 42.2	O9III	FH	13.33	-	FH	0.07	LWRS	1	14.7
P11750	..... HD37026	05 30 12.2	-67 26 08.4	WC4	T88	13.60	-0.31	F83	0.08	LWRS	1	8.6
P21703	..... B1184	05 30 30.6	-71 02 31.3	B0.5V	M02	13.84	-0.08	M02	0.20	LWRS	1	11.8
B12810	..... SK-67 150	05 30 31.8	-67 00 53.2	B0.7Ia	F88	12.24	-	FH	0.06	LWRS	1	7.9
D13803	..... NGC2004-B15	05 30 36.5	-67 17 42.3	B2III	FH	14.18	-	FH	0.06	MDRS	1	11.1
Z90506	..... SK-71 38	05 30 38.7	-71 01 47.9	WC5+OB	FH	13.10	-	FH	0.10	LWRS	1	9.7
D09805	..... SK-71 41	05 30 40.2	-71 05 37.2	O8.5I	M02	12.82	-0.07	M02	0.15	MDRS	1	10.0
C16007	..... SK-66 118	05 30 44.6	-66 52 38.9	B2Ia	F88	11.81	-	FH	0.11	LWRS	1	12.4
D13804	..... NGC2004-B30	05 30 47.6	-67 17 22.8	B1III	FH	13.83	-	FH	0.06	MDRS	1	11.9
B12805	..... HD269668	05 31 00.9	-68 53 56.7	BN1Ia	F91	12.01	-	FH	0.09	LWRS	1	3.9
P10315	..... SK-71 45	05 31 15.5	-71 04 08.9	O4-5III(f)	W77	11.51	-0.19	H91	0.20	LWRS	4	18.8
P11748	..... HDE269687	05 31 25.6	-69 05 38.4	WN1Ih	C97	11.90	-0.07	I75	0.10	LWRS	1	3.8

TABLE 1 (Continued)

<i>FUSEID</i> <sup>a</sup>	Object Name <sup>b</sup>	R.A. (J2000)	Decl. (J2000)	Sp. Type	Sp. Type Ref. <sup>d</sup>	<i>V</i>	( <i>B</i> - <i>V</i> )	Photo Ref. <sup>d</sup>	<i>E</i> ( <i>B</i> - <i>V</i> )	Aperture <sup>c</sup>	Num DS <sup>e</sup>	Exp. Time <sup>a</sup> (ks)
E51137	SK-67 161	05 31 32.9	-67 40 46.6	WN4b	M02	14.53	-0.17	M02	0.07	LWRS	3	30.9
A13301	SK-67 166	05 31 44.3	-67 38 00.6	O4If+	W77	12.27	-0.22	A72	0.10	LWRS	63	222.0
D09806	SK-71 46	05 31 50.0	-71 03 40.0	O4If	M95	13.25	-	FH	0.15	MDRS	1	6.5
P10316	SK-67 169	05 31 51.6	-67 02 22.3	B1Ia	F88	12.18	-0.12	I75	0.20	LWRS	1	39.1
P11719	SK-67 167	05 31 51.9	-67 39 41.1	O4Inf+	G87a	12.54	-0.19	I75	0.14	LWRS	2	10.2
B08609	SK-67 168	05 31 52.1	-67 34 20.8	O8Iaf	F88	12.08	-0.17	F88	0.14	MDRS	1	4.1
D09801	SK-67 174	05 32 11.3	-67 41 16.0	O8V	M95	11.52	-	FH	0.10	MDRS	1	2.8
E51138	B1196	05 32 19.2	-67 49 50.1	O9V	M02	14.53	-0.23	M02	0.07	LWRS	1	21.4
D09802	SK-67 176	05 32 27.4	-67 41 13.3	O7Ib(f)	F88	11.66	-	FH	0.10	MDRS	1	4.7
B09001	SK-67 181	05 32 48.0	-67 20 42.0	B0.5	M02	12.19	-0.12	M02	0.20	LWRS	1	7.9
A04401	4U0532-664	05 32 49.5	-66 22 13.5	O8IV	FH	14.00	-	FH	0.05	LWRS	1	49.1
Z90504	SK-67 184	05 33 11.3	-67 42 45.0	WN4o+B	M02	13.13	-0.13	M02	0.10	LWRS	1	4.5
P11731	SK-67 191	05 33 34.1	-67 30 19.6	O8V	C86	13.46	-0.21	I79	0.10	LWRS	2	15.0
B07703	HV5936	05 33 39.0	-66 37 39.8	B2V	FH	14.80	-	FH	0.07	LWRS	1	24.9
P11727	B1208	05 33 57.4	-67 24 20.0	O7Vz	W02b	13.96	-0.24	I82	0.03	LWRS	4	15.6
C16010	SK-67 199	05 34 18.5	-67 18 13.3	B3Ia	F88	11.06	-	FH	0.13	LWRS	1	11.4
P11751	HD37680	05 34 19.3	-69 45 10.0	WC4	T88	13.35	-0.20	F83	0.05	LWRS	1	7.0
F32103	J053441-693139	05 34 41.3	-69 31 39.0	O2-O3.5If*	W02a	13.70	-	FH	0.00	LWRS	1	28.3
E51139	SK-67 205	05 34 52.9	-67 16 20.6	O8V	M02	13.72	-0.21	M02	0.09	MDRS	2	16.8
P11716	HD269810	05 35 13.9	-67 33 27.0	O2III(†*)	W02a	12.28	-0.23	A72	0.14	LWRS	2	14.9
P21304	SN1987A-STAR2	05 35 27.7	-69 16 08.8	SNR	FH	15.10	-	FH	0.16	MDRS	1	44.6
P21303	SN1987A-STAR3	05 35 28.4	-69 16 11.8	B0V	FH	15.80	-	FH	0.16	MDRS	1	60.8
P11728	B1229	05 35 32.2	-66 02 37.6	O7V-III	W02b	12.95	-0.17	B75	0.15	MDRS	1	4.5
Z90510	Brey64	05 35 54.4	-68 59 07.4	WN9h	M02	13.21	+0.06	M02	0.10	LWRS	1	13.6
E51140	B1237	05 36 14.6	-67 39 19.3	O3V	M02	13.89	-0.12	M02	0.18	LWRS	1	36.6
B08605	SK-68 129	05 36 26.8	-68 57 31.9	B1I	M02	12.78	+0.03	M02	0.34	LWRS	1	6.7
Z90507	SK-69 220	05 36 43.8	-69 29 47.4	OlaIpe	W77	10.58	-	FH	0.10	LWRS	1	2.5
P11738	SK-66 169	05 36 54.5	-66 38 25.0	O9.7Ia+	F88	11.56	-0.13	R78	0.16	LWRS	1	5.2
P21502	HD38029	05 36 56.0	-69 11 36.0	O	FH	11.59	-	FH	0.42	LWRS	2	27.7
E51141	SK-66 171	05 37 02.4	-66 38 39.0	O9Ia	F88	12.19	-	FH	0.15	LWRS	1	1.3
P11722	SK-66 172	05 37 05.5	-66 21 35.7	O2III(†*)+OB	W02a	13.13	-0.12	R78	0.21	LWRS	1	3.6
B08604	SK-69 228	05 37 09.2	-69 20 19.5	BC1.5Ia	F91	11.93	-	FH	0.25	LWRS	1	9.4
C00206	B1253	05 37 34.4	-69 01 09.8	O3V	M02	13.76	-0.09	M02	0.25	LWRS	2	22.2
P11739	SK-68 135	05 37 48.6	-68 55 08.0	ON9.7Ia+	W77	11.36	0.00	A72	0.25	LWRS	1	7.1
B12807	SK-69 237	05 38 01.3	-69 22 13.7	B1Ia	F91	12.08	-	FH	0.14	LWRS	1	5.0
E51142	SK-68 137	05 38 24.7	-68 52 32.8	O3III*	M02	13.29	-0.07	M02	0.23	LWRS	1	36.5
D09817	Mk42	05 38 42.1	-69 05 54.7	O3II*/WN6-A	W97	10.96	+0.12	F83	0.40	MDRS	1	3.7
D09816	SK-69 243	05 38 42.5	-69 06 03.2	WN5+OB	M98	9.50	+0.13	F83	0.40	MDRS	1	4.4
P10318	SK-69 246	05 38 53.5	-69 02 00.7	WN6h	S96	11.16	-0.16	F83	0.25	LWRS	1	22.5
B08606	SK-68 140	05 38 57.3	-68 56 52.9	B0:	M02	12.79	+0.05	M02	0.33	LWRS	1	10.7
P11746	HDE269927	05 38 58.2	-69 29 19.1	WN9h	S96	12.63	-0.13	T98	0.19	LWRS	1	7.2

TABLE 1 (Continued)

FUSEID <sup>a</sup>	Object Name <sup>a</sup>	R.A. (J2000)	Decl. (J2000)	Sp. Type	Sp. Type Ref. <sup>d</sup>	V	(B - V)	Photo Ref. <sup>d</sup>	E(B - V)	Aperture <sup>e</sup>	Num DS <sup>e</sup>	Exp. Time <sup>a</sup> (ks)
X01801	..... Sand 2	05 39 34.4	-68 44 09.5	WO3	FH	16.20	-	FH	0.15	LWRS	1	8.1
P21701	..... SK-69 257	05 39 58.9	-69 44 03.2	O9II	FH	12.53	-	FH	0.20	LWRS	1	10.9
E95705	..... HD38489	05 40 13.4	-69 22 46.2	B0	FH	13.86	-	FH	0.00	MDRS	1	5.7
A04912	..... SK-71 50	05 40 43.3	-71 28 59.3	O6.5II	C86	13.44	-0.12	R78	0.20	LWRS	1	5.4
B08608	..... SK-69 279	05 41 44.7	-69 35 14.7	O9I	FH	11.93	-	FH	0.36	LWRS	1	6.0
A04909	..... SK-66 185	05 42 30.5	-66 18 10.7	B0Iab	C86	13.11	-0.19	179	0.05	LWRS	1	7.0
B08607	..... SK-68 155	05 42 54.9	-68 56 54.4	O8I	FH	12.72	-	FH	0.34	LWRS	1	8.0
D09814	..... D301-1005	05 43 08.3	-67 50 52.4	O9.5V	M02	14.11	-0.23	M02	0.10	MDRS	1	16.6
D09811	..... LH114-7	05 43 12.8	-67 51 16.2	O3III(f)*	M02	13.66	-0.25	M02	0.10	MDRS	1	12.9
D09812	..... SK-67 250	05 43 15.4	-67 51 09.6	O7.5II(f)	M95	12.68	-	FH	0.10	MDRS	1	2.6
D09815	..... D301-NW8	05 43 15.9	-67 49 51.0	O8V	M02	14.37	-0.22	M02	0.10	MDRS	1	13.4
P11729	..... BI272	05 44 23.1	-67 14 29.3	O7:III-II:	W02b	13.28	-0.22	182	0.17	LWRS	2	10.9
B12802	..... SK-67 256	05 44 25.1	-67 13 49.4	BC1Ia	F91	11.90	-0.08	F88	0.09	LWRS	1	3.9
C14002	..... SK-69 297	05 44 31.3	-69 20 15.5	WN1Ih	FH	12.73	-	FH	0.26	LWRS	1	16.6
B09002	..... SK-67266	05 45 52.0	-67 14 25.0	O8	FH	12.01	-	FH	0.19	LWRS	1	4.7
P11726	..... SK-70 115	05 48 49.7	-70 03 57.5	O6.5Iaf	Wpc	12.24	-0.10	175	0.22	LWRS	1	5.2
A04908	..... SK-68 171	05 50 22.7	-68 11 26.4	B0:7Ia	F91	12.01	-0.09	A72	0.10	LWRS	1	4.6
A04910	..... SK-70 120	05 51 20.8	-70 17 08.7	B1Ia	F88	11.59	-0.06	A72	0.14	LWRS	2	7.1
A04911	..... SK-69 305	05 54 12.7	-69 29 55.6	B5Ia	J01	13.05	-	FH	0.05	LWRS	1	5.8

<sup>a</sup>FUSE ID indicates the FUSE program and target identifier used in the online atlas. Column headed Num DS indicates those objects for which multiple data sets have been combined. In these cases, the FUSE ID shows the dominant or longest individual observation. Total exposure time summed is in the Exp. Time column. In the online atlas, the Num DS column links to a listing showing the individual data sets that were combined.

<sup>b</sup>To avoid formatting problems here, the names of objects from the OGLE survey have been shortened from those shown on the web page.

<sup>c</sup>The aperture characteristics are defined in the text.

<sup>d</sup>Spectral Type and Photometry References: A72—Ardeberg et al. 1972; A75—Azzopardi et al. 1972; A77—Ardeberg & Maurice 1977; A79—Azzopardi & Vigneau 1979; B75—Brunet et al. 1975; C82—Crampton & Greasley 1982; C86—Conti et al. 1986; C97—Crowther & Smith 1997; C98—Crowther et al. 1998; F83—Feitzinger & Isserstedt 1983; F88—Fitzpatrick 1988; F91—Fitzpatrick 1991; FH—FUSE fits file header; G87a—Garmany & Walborn 1987; G87b—Garmany et al. 1987; H91—Heydari-Malayeri & Hutsemekers 1991; I75—Isserstedt 1975; I78—Isserstedt 1978; I79—Isserstedt 1979; I82—Isserstedt 1982; J01—Jaxon et al. 2001; K94—Koenigsberger et al. 1994; L97—Lennon 1997; M89—Massey et al. 1989; M90—Moffat et al. 1990; M95—Massey et al. 1995; M98—Massey & Hunger 1998; M01—Massey & Duffy 2001; M02—Massey 2002; P92—Parker et al. 1992; R78—Rousseau et al. 1978; § 96—Smith et al. 1996; T88—Torres-Dodgen & Massey 1988; T98—Testor & Niemela, 1998; W77—Walborn 1977; W82—Walborn 1982; W83—Walborn 1983; W86—Walborn & Blades 1986; W95—Walborn et al. 1995; W97—Walborn & Blades 1997; W00—Walborn et al. 2000; W02a, W02b—Walborn et al. (2002a, 2002b); Wpc—Walborn private communication; Z02—Zaritsky et al. 2002.

TABLE 2  
FUSE SMC OBJECTS AND INFORMATION

FUSE ID <sup>a</sup>	Object Name <sup>b</sup>	R.A. (J2000)	Decl. (J2000)	Sp. Type	Sp. Type Ref. <sup>d</sup>	V	(B - V)	Photo Ref. <sup>d</sup>	$E(B - V)$	Aperture <sup>e</sup>	Num DS <sup>a</sup>	Exp. Time <sup>a</sup> (ks)
F90702	.....	00 43 36.9	-73 26 37.7	B2V	FH	14.18	-	FH	0.06	LWRS	1	30.6
P22101	OGLE004336.91-732637	00 45 18.2	-73 15 23.4	O9III	L97	13.46	+0.03	A75	0.33	LWRS	1	4.0
G03906	SMC-WR10-POS2	00 45 27.5	-73 04 50.1	WN3+abs	M01	15.76	-0.08	M01	0.22	LWRS	1	26.5
P11753	AV14	00 46 32.6	-73 06 05.6	O3-4V	G87b	13.77	-0.19	A75	0.13	LWRS	1	6.8
F90701	OGLE004633.76-731204	00 46 33.7	-73 12 04.3	B2V	FH	14.06	-	FH	0.06	LWRS	1	30.5
P11501	AV15	00 46 42.1	-73 24 54.7	O6.5II(f)	W00	13.17	-0.21	I78	0.00	LWRS	1	16.2
E51101	AV16	00 46 54.9	-73 08 33.4	B1LBV	FH	13.03	+0.13	Z02	0.22	LWRS	1	33.7
B08901	AV18	00 47 13.1	-73 06 24.8	B2Ia	L97	12.48	-	FH	0.21	LWRS	2	51.3
D16207	AV22	00 47 38.7	-73 07 48.4	B5Ia	L97	12.25	-	FH	0.05	LWRS	1	24.1
P11760	AV26	00 47 50.0	-73 08 20.7	O7III	G87b	12.55	-0.20	A75	0.11	LWRS	1	4.0
G03903	SMC-WR2	00 48 30.8	-73 15 45.0	WN5+O	FH	14.23	-	FH	0.15	LWRS	1	9.8
P11502	AV47	00 48 51.3	-73 25 57.6	O8III(f)	W00	13.38	-0.26	A75	0.00	LWRS	1	16.2
G03904	SMC-WR3	00 49 59.3	-73 22 13.6	WN3+	M02	14.48	-0.12	M02	0.20	LWRS	1	13.6
E51102	AV61	00 50 01.7	-72 11 26.0	O5V	M02	13.54	-0.18	M02	0.12	LWRS	1	12.9
P11503	AV69	00 50 17.4	-72 53 29.9	OC7.5III((f))	W00	13.35	-0.22	A75	0.00	LWRS	1	17.5
B09006	AZV70	00 50 18.1	-72 38 09.8	O9.5Iw	W83	12.38	-0.17	A75	0.15	LWRS	3	10.3
F92701	AV73	00 50 27.9	-73 30 16.9	O8.5V	M95	14.08	-	FH	0.10	LWRS	1	17.1
P11504	AV75	00 50 32.5	-72 52 36.2	O5III(f+)	W00	12.79	-0.16	I78	0.00	LWRS	1	14.4
P21708	AV81	00 50 43.4	-73 27 06.1	WN5h	S96	13.29	-0.10	A75	0.11	LWRS	2	14.5
E51117	AV80	00 50 43.9	-72 47 40.8	O7III	M02	13.32	-0.13	M02	0.17	LWRS	1	18.5
P11762	AV83	00 50 52.0	-72 42 14.5	O7Iaf+	W00	13.58	-0.13	W00	0.12	LWRS	1	4.0
F90703	OGLE005100.18-725303	00 51 00.1	-72 53 03.9	B2V	FH	13.56	-0.01	Z02	0.06	LWRS	1	26.1
E05401	AV95	00 51 21.6	-72 44 14.4	O7III((f))	W00	13.91	-0.30	A75	0.06	LWRS	2	59.5
C16001	AV96	00 51 22.9	-72 07 20.2	B2I	M02	12.59	-0.10	M02	0.03	LWRS	1	8.1
D16201	AV104	00 51 38.5	-72 48 05.5	B0Ia	M02	13.17	-0.16	M02	0.05	LWRS	1	8.1
E51103	AV120	00 52 15.1	-72 09 15.3	O9V	M02	14.56	-0.23	M02	0.07	LWRS	3	35.6
Z91221	AV119	00 52 15.7	-73 10 46.1	B2II	FH	13.74	-0.13	Z02	0.00	LWRS	1	9.0
E51104	AV135	00 52 49.5	-72 08 26.6	O7III	M02	13.96	-0.23	M02	0.07	LWRS	1	27.3
G03905	SMC-WR9	00 54 32.1	-72 44 35.6	WN3	M02	15.24	-0.12	M02	0.17	LWRS	1	17.2
F92702	HV1620	00 54 38.6	-72 30 04.2	O9V+O9.5III	FH	14.08	-	FH	0.12	LWRS	1	9.4
P21707	AV170	00 55 42.4	-73 17 30.0	O9.7III	W00	14.09	-0.23	A75	0.07	LWRS	1	8.8
G07601	NGC330-B30	00 56 09.4	-72 27 58.9	B3III	FH	14.22	-0.13	Z02	0.15	LWRS	1	12.4
G07602	NGC330-B12	00 56 25.5	-72 27 09.0	B2IIe	FH	15.38	-	FH	0.15	LWRS	1	7.3
Z91220	AV175	00 56 38.0	-72 36 34.8	B1IIW	M02	13.53	-0.08	M02	0.00	LWRS	1	6.9
C00201	AV177	00 56 44.1	-72 03 31.6	O5V	M02	14.53	-0.21	M02	0.15	LWRS	2	18.0
C16004	AV187	00 57 31.6	-71 19 58.9	B3Ia	L97	12.62	-0.80	Z02	0.01	LWRS	1	24.6
F90704	OGLE005745.25-723532	00 57 45.2	-72 35 32.0	B2V	FH	13.82	-	FH	0.06	LWRS	1	1.7
B13402	NGC346-12	00 58 14.1	-72 10 46.3	O9.5-B0V	W00	14.87	-	FH	0.16	MDRS	1	13.9
D13801	NGC346-11	00 58 14.2	-72 09 18.4	B0V	FH	15.28	-	FH	0.14	LWRS	1	37.4
P22103	AV208	00 58 33.1	-72 39 31.6	O8V	M95	14.10	+0.01	A75	0.32	LWRS	1	7.6
P11759	AV207	00 58 33.1	-71 55 46.5	O7V	C82	14.37	-0.22	A75	0.10	LWRS	1	3.8

TABLE 2 (Continued)

FUSE ID <sup>a</sup>	Object Name <sup>b</sup>	R.A. (J2000)	Decl. (J2000)	Sp. Type	Sp. Type Ref. <sup>d</sup>	V	(B - V)	Photo Ref. <sup>d</sup>	E(B - V)	Aperture <sup>e</sup>	Num DS <sup>c</sup>	Exp. Time <sup>a</sup> (ks)
D16206	AV210	00 58 35.7	-72 16 24.9	B3I	M02	12.60	-0.02	M02	0.11	LWRS	1	22.5
D16204	AV215	00 58 55.6	-72 32 08.1	B3I	M02	12.69	-0.09	M02	0.07	LWRS	1	10.7
P20305	NGC346-6	00 58 57.7	-72 10 33.6	O4V((f))	W05	14.02	-0.24	M89	0.09	MDRS	2	10.6
D16205	AV216	00 58 59.1	-72 44 33.7	B0IIW	M02	14.22	-0.13	M02	0.10	LWRS	1	11.7
P20304	NGC346-4	00 59 00.3	-72 10 37.9	O5-6V	W86	13.66	-0.23	M89	0.10	MDRS	1	11.4
P20303	NGC346-3	00 59 01.0	-72 10 28.2	O3III(f)	W02a	13.50	-0.23	M89	0.10	MDRS	1	8.0
P20302	NGC346-1	00 59 04.8	-72 10 24.8	O4III(n)(f)	W86	12.57	-0.23	M89	0.13	MDRS	1	4.5
P21704	AV220	00 59 10.1	-72 05 48.1	O6.5?fp	W00	14.50	-0.22	A75	0.10	LWRS	1	11.1
C15801	NGC346-637	00 59 14.6	-72 11 58.8	B0V	FH	14.71	+2.49	Z02	0.14	MDRS	1	21.9
P22301	HD5980	00 59 26.5	-72 09 53.9	WN	K94	11.86	-0.26	A75	0.07	LWRS	15	93.7
P10302	SK80	00 59 31.9	-72 10 45.8	O7Iaf+	W77	12.36	-0.20	A75	0.15	LWRS	2	22.0
P10303	SK82	00 59 45.7	-72 44 56.1	B0Iaw	W83	12.20	-0.18	A75	0.15	LWRS	1	16.2
P11766	AV238	00 59 55.6	-72 13 37.7	O9.5III	W00	13.77	-0.22	A75	0.08	LWRS	1	11.1
P11758	AV243	01 00 06.8	-72 47 19.0	O6V	W95	13.87	-0.22	A75	0.10	LWRS	1	4.6
P11769	AV242	01 00 06.8	-72 13 57.0	B0.7Iaw	W85	12.11	-0.13	A75	0.03	LWRS	1	5.0
E51105	AV255	01 00 42.1	-71 31 13.3	O8V	M95	12.80	-	FH	0.09	LWRS	1	7.3
E51106	AV261	01 00 58.7	-72 30 49.7	O8.5I	M02	13.88	-0.07	M02	0.23	LWRS	1	16.9
P11770	AV264	01 01 07.7	-71 59 58.6	B1Ia	L97	12.36	-0.15	A75	0.03	LWRS	1	4.3
Z91223	AV266	01 01 09.3	-72 27 28.2	B1III	M02	12.55	-0.12	M02	0.13	LWRS	1	10.0
E51107	AV267	01 01 15.6	-72 06 35.4	O8Vn	M02	14.84	-0.26	M02	0.05	MDRS	1	35.0
B09007	Sk101	01 01 54.0	-72 12 00.0	O9.5I	FH	12.86	-	FH	0.27	LWRS	1	5.4
C15802	AV304	01 02 21.4	-72 39 14.6	B0.5V	C82	14.98	-0.20	C82	0.08	LWRS	1	18.2
P11506	AV321	01 02 57.0	-72 08 09.3	B0IIWw	G87b	13.88	-0.21	A75	0.00	LWRS	1	16.9
P11764	AV327	01 03 10.5	-72 02 13.8	O9.5I-Ibw	W00	13.25	-0.22	A79	0.09	LWRS	1	4.2
F32101	H53-47	01 03 22.0	-72 05 38.3	O6V+O4III	FH	13.60	-	FH	0.00	MDRS	4	108.5
P10304	SK108	01 03 25.2	-72 06 43.3	O6.5(m)+WN3	W77	12.41	-0.29	A75	0.15	MDRS	1	12.8
E51108	AV334	01 03 26.4	-72 57 02.5	O8.5V	FH	13.78	-	FH	0.15	MDRS	2	25.5
P24301	AV336a	01 03 35.5	-72 03 21.8	WN2+abs	M02	12.96	-0.06	M02	0.09	LWRS	1	9.2
C16005	AV362	01 04 49.1	-72 06 22.0	B3Ia	L97	11.36	-	FH	0.11	LWRS	1	9.1
P11765	AV372	01 04 55.7	-72 46 47.7	O9.5Iabw	W02b	12.63	-0.18	A75	0.13	LWRS	1	4.3
C16002	AV374	01 05 01.6	-72 26 53.3	B1	M02	13.04	-0.13	M02	0.00	LWRS	1	8.8
B13401	AV377	01 05 07.3	-72 48 18.3	O6V	FH	14.59	-0.25	Z02	0.02	LWRS	1	18.4
P11507	AV378	01 05 09.4	-72 05 35.0	O8V	G87b	13.88	-0.24	A75	0.00	LWRS	1	14.7
P11754	AV388	01 05 39.6	-72 29 26.8	O4V	M02	14.09	-0.21	M02	0.11	LWRS	1	5.3
B13404	AV393	01 05 56.3	-72 19 44.8	B3Ia	FH	11.43	-	FH	0.10	LWRS	1	7.9
P11767	AV423	01 07 40.4	-72 50 59.6	O9.5II(n)	W02b	13.28	-0.19	A75	0.11	LWRS	1	3.5
E51116	AV435	01 08 17.8	-71 59 54.3	O4V	M02	14.00	-0.06	M02	0.20	LWRS	1	35.4
E51109	AV440	01 08 56.0	-71 52 46.5	O7V	M02	14.48	-0.18	M02	0.12	LWRS	1	36.7
E51110	AV446	01 09 25.4	-73 09 29.7	O6.5V	M02	14.59	-0.24	M02	0.06	LWRS	1	27.1
P21706	AV451	01 10 25.9	-72 23 28.3	O9V	G87b	14.15	-0.23	A75	0.08	LWRS	1	6.5
Q10701	AV456	01 10 55.7	-72 42 55.6	O9.5V	M02	12.83	+0.10	M02	0.40	LWRS	6	26.9
P21705	AV461	01 11 25.4	-72 09 48.5	O8V	G87b	14.66	-0.31	I78	0.00	LWRS	1	7.0

TABLE 2 (Continued)

<i>FUSE</i> ID <sup>a</sup>	Object Name <sup>b</sup>	R.A. (J2000)	Decl. (J2000)	Sp. Type	Sp. Type Ref. <sup>d</sup>	<i>V</i>	( <i>B</i> - <i>V</i> )	Photo Ref. <sup>d</sup>	<i>E</i> ( <i>B</i> - <i>V</i> )	Aperture <sup>e</sup>	Num DS <sup>c</sup>	Exp. Time <sup>a</sup> (ks)
A11803	.....	AZV462	01 11 25.8	-72 31 21.0	B1	M02	12.54	-0.13	M02	LWRS	1	5.2
P11763	.....	AV469	01 12 28.9	-72 29 28.8	O8.5II(f)	W02b	13.20	-0.22	A75	LWRS	1	8.2
C16003	.....	AV472	01 13 01.8	-72 45 47.6	B2	M02	12.62	-0.11	M02	LWRS	1	16.8
C00203	.....	AV476	01 13 42.4	-73 17 29.6	O6.5V	M02	13.52	-0.09	M02	LWRS	1	21.6
B08902	.....	Sk155	01 14 50.0	-73 20 17.0	O9Ib	L97	12.50	-	FH	LWRS	1	12.8
E51112	.....	AV480	01 14 55.0	-72 21 38.1	Oe	M02	14.34	-0.03	M02	LWRS	1	26.0
B13403	.....	AV483	01 15 28.8	-73 19 49.8	B1.5I	FH	11.85	-	FH	LWRS	1	14.8
B02702	.....	Sk157	01 15 51.9	-73 20 48.6	O9.5:III	M02	12.07	-0.19	M02	LWRS	1	3.3
P11768	.....	SK159	01 15 58.8	-73 21 24.1	B0.5Iaw	W83	11.89	-0.13	A77	LWRS	4	19.8
D17501	.....	SMC-X-1	01 17 05.2	-73 26 35.9	B0I	FH	13.80	-	FH	LWRS	3	224.0
E51113	.....	AV491	01 17 16.8	-73 10 01.1	O7.5III:	M02	14.72	-0.20	M02	LWRS	1	22.8
Z91224	.....	AV506	01 22 11.1	-73 26 51.8	B0	M02	13.53	-0.17	M02	LWRS	1	12.7
A12302	.....	SK188	01 31 04.2	-73 25 02.2	WO3+O4V	C98	12.41	-0.29	A75	LWRS	22	84.2
E51114	.....	SK190	01 31 28.0	-73 22 14.6	O8Iaf	M02	13.54	-0.18	M02	LWRS	1	13.9
D16202	.....	SK191	01 41 42.0	-73 50 38.2	B1.5Ia	L97	11.86	-	FH	LWRS	1	11.1
E51115	.....	SK197	01 50 22.6	-74 07 13.8	O8.5Ve	FH	13.38	-	FH	LWRS	1	26.2
P24101	.....	DI1388	02 57 11.9	-72 52 54.6	B0V	FH	14.39	-	FH	LWRS	1	16.7

<sup>a</sup>*FUSE* ID indicates the *FUSE* program and target identifier used in the online atlas. The 'Num DS' column indicates those objects for which multiple data sets have been combined. In these cases, the *FUSE* ID shows the dominant or longest individual observation. The total exposure time summed is indicated in the 'Exp. Time' column. In the online atlas, the 'Num DS' column links to a listing showing the individual data sets that were combined.

<sup>b</sup>To avoid formatting problems here, the names of objects from the OGLE survey have been shortened from those shown on the web page.

<sup>c</sup>The aperture characteristics are defined in the text.

<sup>d</sup>Spectral Type and Photometry References: A72—Ardeberg et al. 1972; A75—Azzopardi et al. 1975; A77—Ardeberg & Maurice 1977; A79—Azzopardi & Vigneau 1979; B75—Brunet et al. 1975; C82—Crampton & Greasley 1982; C86—Conti et al. 1986; C97—Crowther & Smith 1997; C98—Crowther et al. 1998; F83—Feitzinger & Isserstedt 1983; F88—Fitzpatrick 1988; F91—Fitzpatrick 1991; FH—*FUSE* fits file header; G87a—Garmany & Walborn 1987; G87b—Garmany et al. 1987; H91—Heydari-Malayeri & Hutsemekers 1991; I75—Isserstedt 1975; I78—Isserstedt 1978; I79—Isserstedt 1979; I82—Isserstedt 1982; J01—Jaxon et al. 2001; K94—Koenigsberger et al. 1994; L97—Lennon 1997; M89—Massey et al. 1989; M90—Moffat et al. 1990; M95—Massey et al. 1995; M98—Massey & Hunger 1998; M01—Massey & Duffy 2001; M02—Massey 2002; P92—Parker et al. 1992; R78—Rousseau et al. 1978; § 96—Smith et al. 1996; T88—Torres-Dodgen & Massey 1988; T98—Testor & Niemela, 1998; W77—Walborn 1977; W82—Walborn 1982; W83—Walborn 1983; W86—Walborn & Blades 1986; W95—Walborn et al. 1995; W97—Walborn & Blades 1997; W00—Walborn et al. 2000; W02a, W02b—Walborn et al. (2002a, 2002b); Wpc—Walborn private communication; Z02—Zaritsky et al. 2002.

temporal variability, either within individual observations or between one observation and another, will be better served by the products available directly from the standard MAST/FUSE data archive.

### 3. DATA SUMMARIES AND CONTEXT IMAGES

With the reprocessed data in hand, one still has to address how to provide access and insight into the value of a given data set for a particular scientific purpose. We address this by defining a consistent, standardized set of products for each object that provide an overview of each sight line quickly and effectively.

#### 3.1. Lines from the ISM

We have defined a set of interstellar absorption lines that arise in the neutral, warm, and highly ionized phases of the ISM; that span a range of line strengths; and that are located in regions of the spectrum that typically show the least problems with contamination from stellar photospheric lines. The selected lines and relevant parameters are summarized in Table 3. The lines selected to show in the atlas were vetted in part by community input that took place via a preliminary presentation at the conference *Astrophysics in the Far Ultraviolet: Five Years of Discovery with FUSE*, which took place in Victoria, BC, Canada in 2004 August (see Blair et al. 2006). As Table 3 provides the details, we will use approximated wavelengths (nearest Å) in referring to these lines in the rest of this article.

TABLE 3  
SELECTED ISM TRANSITIONS

Ion	Wavelength (Å)	Ionization Range <sup>a</sup> (eV)	$f_{\lambda}$ <sup>c</sup>
Ar I	1048.219	<15.760	0.263
P II	1152.818	10.486–19.725	0.245
Fe II	1144.938	7.870–16.16	0.106 <sup>d</sup>
Fe III	1122.524	16.16–30.651	0.0544
Si II	1020.699	8.151–16.345	0.0168
H <sub>2</sub> 2-0 R(1)	1077.701	<4.48 <sup>b</sup>	0.00809 <sup>e</sup>
H <sub>2</sub> 8-0 R(3)	1006.417	<4.48 <sup>b</sup>	0.0154 <sup>e</sup>
H <sub>2</sub> 5-0 R(4)	1044.546	<4.48 <sup>b</sup>	0.0162 <sup>e</sup>
C I	945.191	<11.260	0.0152
C II	1036.337	11.260–24.383	0.118
O I	924.950	<13.618	0.00154
O I	1039.230	<13.618	0.00907
C III	977.020	24.383–47.887	0.757
O VI	1031.926	113.90–138.12	0.1325
S IV	1062.664	34.79–47.222	0.00494
Fe II	1125.448	7.870–16.16	0.016 <sup>d</sup>

<sup>a</sup> Ionization potential ranges from Moore (1970) unless otherwise noted.

<sup>b</sup> H<sub>2</sub> dissociation energies Spitzer (1978).

<sup>c</sup>  $f$ -values from Morton (2003) unless otherwise noted.

<sup>d</sup> Howk et al. (2000).

<sup>e</sup> Morton & Dinerstein (1976).

The selected lines have been grouped for display into two sets of eight lines. We have identified the following set of eight primary lines for assessing the neutral and low-ionization ISM, as shown in Figure 3: Ar I  $\lambda$ 1048, P II  $\lambda$ 1153, Fe II  $\lambda$ 1145, Fe III  $\lambda$ 1122, Si II  $\lambda$ 1020, H<sub>2</sub>(R1)  $\lambda$ 1077, H<sub>2</sub>(R3)  $\lambda$ 1006, and H<sub>2</sub>(R4)  $\lambda$ 1045. To broaden the information available for assessing each sight line, a second set of ISM transitions is included in a separate eight-panel stack plot, as shown in Figure 4. These transitions include: C I  $\lambda$ 945, C II  $\lambda$ 1036, O I  $\lambda$ 925, O I  $\lambda$ 1039, C III  $\lambda$ 977, O VI  $\lambda$ 1032, S IV  $\lambda$ 1063, and Fe II  $\lambda$ 1125.

We select a small spectral window around each each line that covers both the rest (Milky Way) and Magellanic velocity ranges, convert the data to a velocity scale, and stack the plots (four panels each in two columns) for easy intercomparison. Each plot spans the range from  $-400$  to  $+600$  km s<sup>-1</sup> from the local standard of rest (LSR) reference point. We adopt much the same strategy as used by Danforth et al. (2002) to label the ISM plots. Each panel is labeled at lower left with the transition of interest. Vertical dotted lines are used to mark the nominal rest velocity positions for Milky Way and Magellanic systems. A top row of labels shows the expected positions of various additional ISM absorption lines at the Milky Way rest frame velocity. A second row of labels (in italics) shows the same transitions but for the appropriate Magellanic Cloud velocity. Of course, for a given object and sight line, the actual absorption lines may be shifted somewhat from this nominal value. Scanning the stack plot makes it clear when a shift of the ISM lines relative to the nominal velocity is present for a given object.

Four of the lines in Figure 3, Ar I, P II, Si II, and Fe II, are indicators of the neutral or cold ISM. The Fe III line strength relative to Fe II is an indicator for the presence of warmer material. Three clean H<sub>2</sub> transitions from different rotational levels of the molecule are also shown. These panels not only indicate whether H<sub>2</sub> is present on a given sight line, but whether one expects to see excited levels. In Figure 3, for example, at the Milky Way velocity strong H<sub>2</sub> lines are seen in all three H<sub>2</sub> panels, while much weaker H<sub>2</sub> is seen at the LMC velocity, and only in the R1 and R3 panels. This information is important not only for understanding the H<sub>2</sub> characteristics of each sight line, but also in interpreting what one sees near other lines, since many of the “contaminating” features that appear near the primary transitions shown in each panel can be from H<sub>2</sub>, as indicated by the labels.

The transitions shown in Figure 4 tend to broaden or corroborate the information derivable from Figure 3. Included here are several strong transitions that are often saturated, especially in the line cores (e.g., C II and C III). Because they are so sensitive, these lines show the full extent in velocity space of absorbing material, and often show weak components that would never be seen in the weaker transitions. The two O I lines have significantly different  $f$ -values from each other, and, along with C I, may be useful as additional diagnostics of the

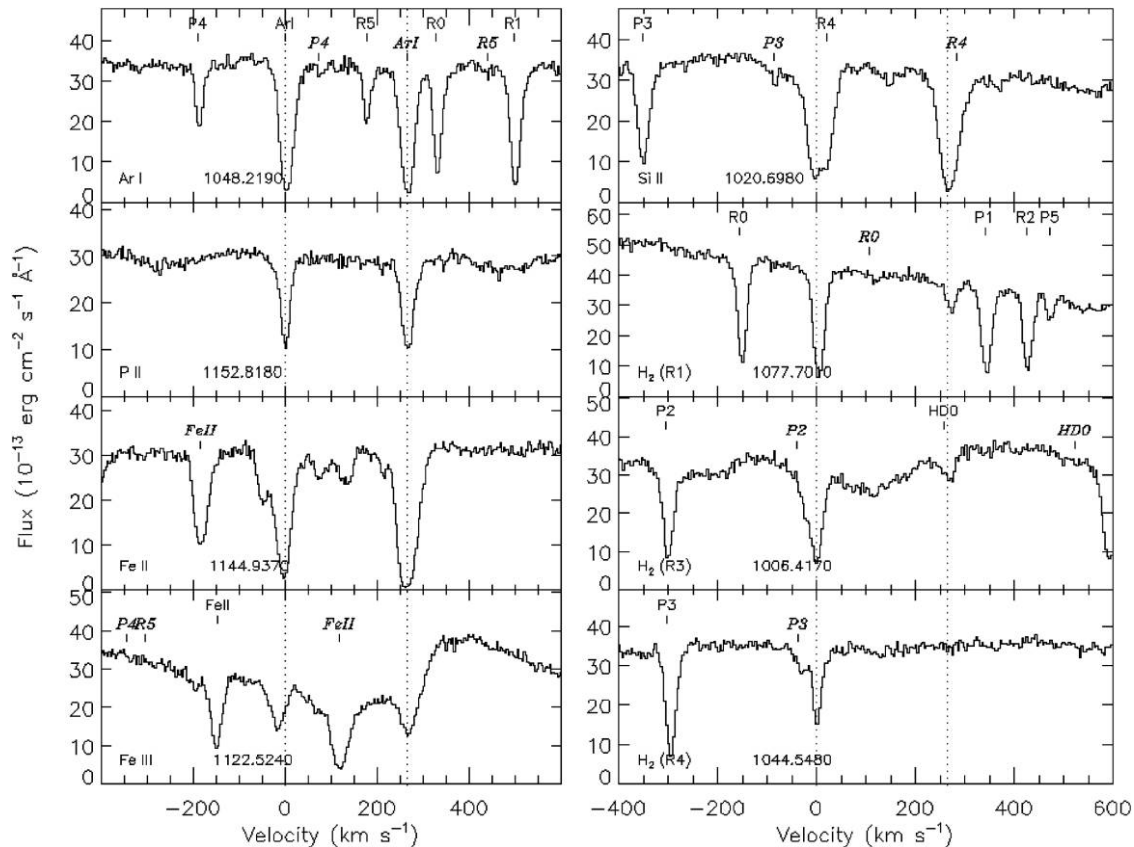


FIG. 3.—Example primary ISM line summary for *FUSE* data set P10310, SK-65°22. Each of the eight panels shows a velocity range from  $-400$   $\text{km s}^{-1}$  to  $600$   $\text{km s}^{-1}$  surrounding the Milky Way rest velocity of the absorption line indicated at the *bottom left* of the panel. Vertical dotted lines indicate the rest velocity of Milky Way (near zero) and relevant Magellanic Cloud, in this case LMC. Line identifications for absorption lines near to the primary transition are also shown. These panels show low-ionization lines and three  $\text{H}_2$  lines from different rotational levels. See text for details.

low-ionization gas in conjunction with lines in Figure 3. S IV and O VI can be used to assess hotter gas along the sight line. In particular, O VI arises from gas near  $300,000$  K in the ISM. When present, it is typically broader than the other ISM lines and is sometimes but not always shifted  $10\text{--}30$   $\text{km s}^{-1}$  toward shorter wavelengths. (O VI is discussed further in § 3.2) Finally, a second Fe II line,  $\lambda 1125$ , is shown for comparison with Fe II  $\lambda 1145$  in the first stack plot. This can be useful as a diagnostic because a stellar feature can sometimes contaminate the region near the  $1145$  Å line. Also,  $\lambda 1125$  has a smaller  $f$ -value and hence does not saturate as readily.

### 3.2. Hot ISM and Stellar Spectrum Overviews

In addition to the ISM velocity plots for each object, we produce an additional two-panel plot as shown in Figure 5. The top panel highlights the  $1028\text{--}1042$  Å spectral region containing both O VI  $\lambda\lambda 1032, 1038$  transitions as well as a number of strong ISM lines such as C II  $\lambda 1036$ , O I  $\lambda 1039$ , and several  $\text{H}_2$  transitions. This panel uses the LiF1 channel of the *\*all\*.fits* or summed *\*all\*.fits* files at full resolution. The O VI lines are

broad and can arise in hot regions of the ISM and/or in the winds and atmospheres of very hot stars, often (but not always) showing a P Cygni line profile. The intent of this panel is to allow the user to assess the features in this spectral region while providing sufficient coverage of the surrounding stellar continuum to make judgments as to what features are stellar and what features are interstellar in origin, especially in comparison with the narrower spectral window shown in Figures 3 and 4. Markers for many of the features expected in this region are shown, with horizontal bars connecting the same transitions at Milky Way rest and (the appropriate) Magellanic rest velocities.

The bottom panel of Figure 5 shows a summary plot of the entire *FUSE* spectral range. This plot uses the NVO (or summed NVO) data file, but bins the data over 20 pixels ( $0.26$  Å). This panel is shown for two reasons: (a) it provides an overview of the stellar spectrum and continuum shape as well as showing the main features in the photospheric spectrum, and (b) it allows a quick assessment of the overall *FUSE* data quality for the object. CalFUSE creates the *\*nvo\*.fits* files by stitching together what it selects as the best available channel data (Dixon et al.

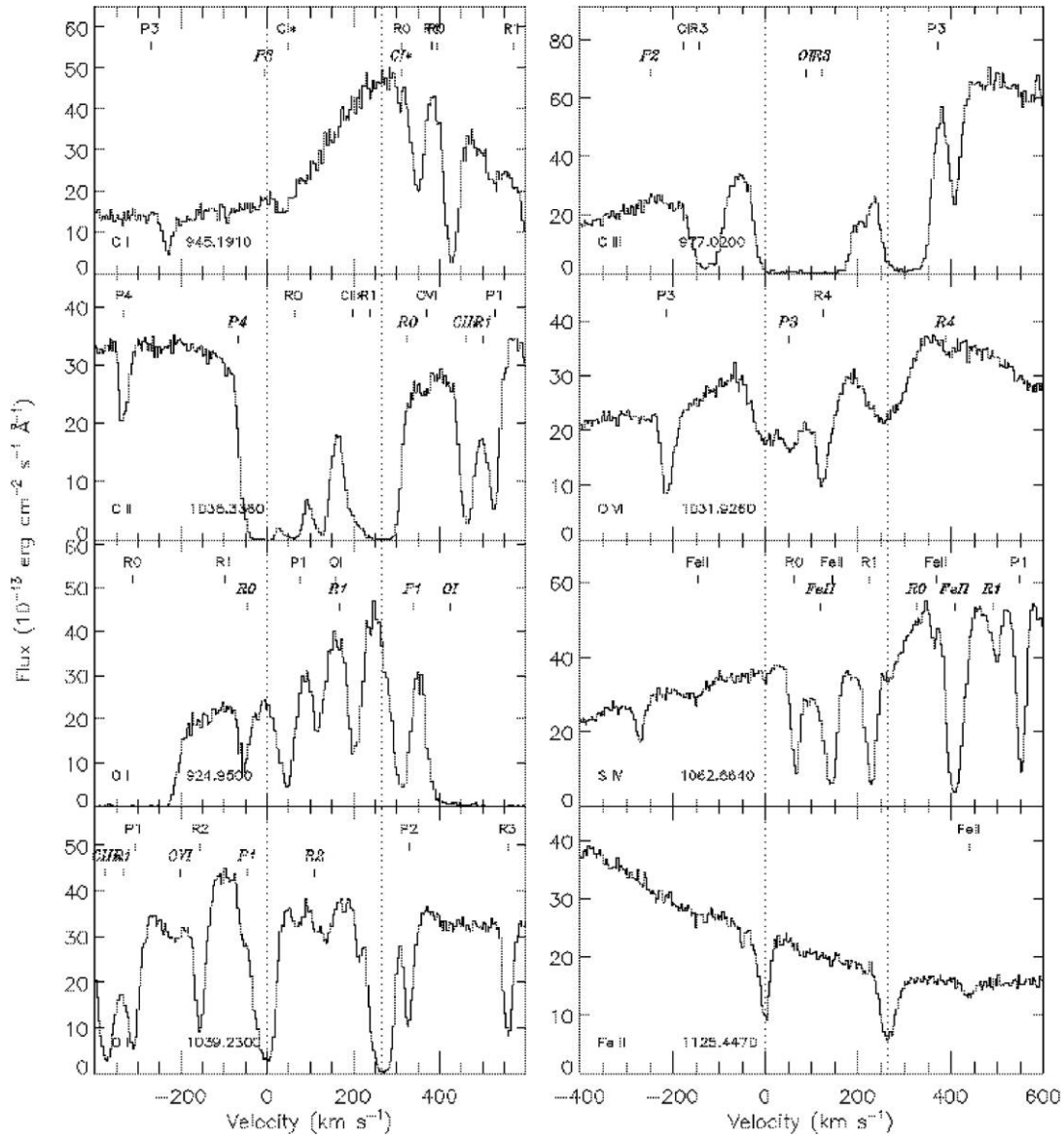


FIG. 4.—Same as Figure 3, but for the secondary set of ISM lines in P10310. This collection of panels shows a number of stronger ISM lines, as well as higher ionization lines such as O VI  $\lambda$ 1031.93 and S IV  $\lambda$ 1062.66. Note that a second Fe II line,  $\lambda$ 1125.45 is shown, for comparison with the  $\lambda$ 1144.94 line in Figure 3.

2007). In a few instances, where little or no data were obtained in a particular channel due to channel alignment issues, a stellar overview plot may have “stair-steps” that are nonphysical. These cases should be obvious when they occur. The full-range *FUSE* spectra serve as a quick look at the stellar spectrum, but the reader is referred to the more detailed *FUSE* MC spectral atlases that have both been published (Walborn et al. 2002; Willis et al. 2004) and placed online as HLSPs at MAST.<sup>12</sup>

<sup>12</sup> See <http://archive.stsci.edu/prepds/atlasfuse/> and [http://archive.stsci.edu/prepds/fuse\\_wratlas/](http://archive.stsci.edu/prepds/fuse_wratlas/) for more information on the stellar features.

### 3.3. Sight Line Context Images

Since nearly every *FUSE* Magellanic Cloud stellar spectrum contains absorption lines due to some component of the host galaxy’s ISM, the question is immediately raised as to whether information about this ISM component is apparent from inspection of data at other wavelengths. To help assess this question we provide optical and infrared context imagery for a 20’ region surrounding each sight line. These are described in detail in the following two subsections. In both optical and IR image displays, we supply ancillary information to enhance the context. For scale, a standardized 1’ box is shown in each frame, centered on the object position. In the optical frames, the object is usually

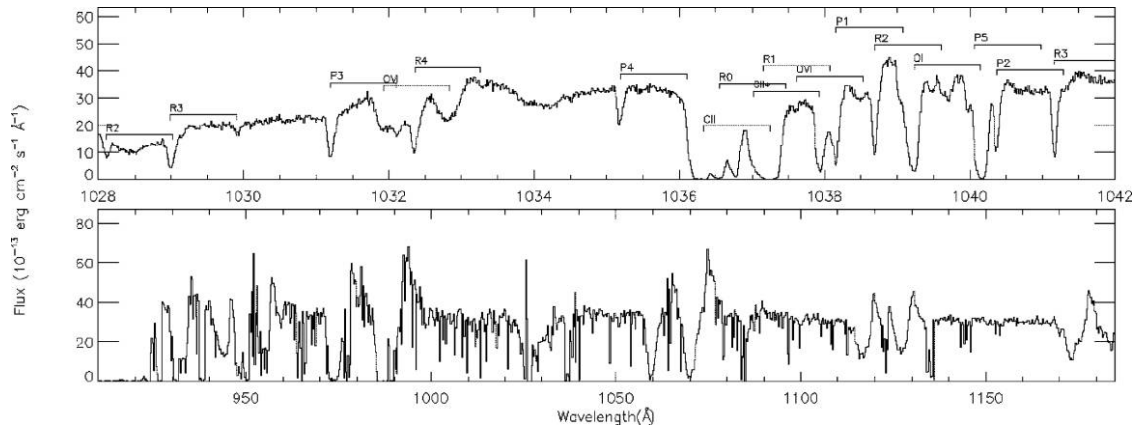


FIG. 5.—Example O VI region and stellar summary plot for the same object used in Figures 3 and 4. The *top panel* shows the 1028–1042 Å region at full resolution. Positions of the O VI doublet and a number of ISM lines in the region are indicated at both Milky Way and Magellanic rest velocities, connected by a bar. The *bottom panel* shows the full *FUSE* spectral range but binned by 20 pixels (0.26 Å), to show an overview of the stellar spectrum. Note the presence of strong broad absorptions and P Cygni profiles that are intrinsic to the spectrum of the star.

visible at the center of the box. This is not always the case for the IR images. In addition, star symbols are drawn at the locations of any other *FUSE* objects within the field of view of a primary sight line so that the potential availability of other data sets along nearly the same direction can be assessed. A coordinate grid is also provided to help identify stars and other features of interest in the fields of view (FOVs).

### 3.3.1. Optical Context Images

At optical wavelengths, we use data from the Magellanic Clouds Emission Line Survey (MCELS, Smith et al. 2004). The MCELS project has obtained full coverage of both Magellanic Clouds at the wavelengths of three key emission lines: H $\alpha$   $\lambda$ 6563, [S II]  $\lambda$ 6725, and [O III]  $\lambda$ 5007; plus red and green continuum bands to allow continuum subtraction (Smith et al. 2005; Winkler et al. 2005). These emission lines provide information on the warm neutral and ionized medium. We use the emission line data without star subtraction in order to show both the target stars and any surrounding nebular emission. The MCELS team provided full galaxy LMC and SMC mosaics in FITS format with World Coordinate System information in place and standardized to a pixel scale of 3.0" per pixel, which made the task of extracting the 20' context images straightforward.

In Danforth et al. (2002), only an H $\alpha$  image was displayed. We have revised the IDL program used by Danforth et al. (2002) to combine the three emission line images into a single color optical context image for each sight line. We show an example in Figure 6, where the three individual emission line frames are shown in black and white along with the color composite. We experimented with various display options with the goal of forcing as much dynamic range into the display as possible. The program automatically assesses the data range in each frame, subtracts the sky level, and then applies a hyperbolic arcsine scaling function (Lupton et al. 2004). As the idea is to provide

the best context information for understanding the *FUSE* data, which sample the pencil beam of ISM directly on the sight line to the object, the program has the capability to sample regions directly adjacent to the object and factor this information into the scaling of the display. Thus, in some cases the overall appearance of a context image may suffer in order to show the region near the object to better advantage. In most cases, the scaling used produces a reasonable overall display.

In each color optical context image, the H $\alpha$  frame is shown in red, the [S II] frame is shown in green, and the [O III] frame is displayed in blue. Stars typically appear white (showing up in all three frames). In addition to these primary colors, their combinations also provide information. Regions of relatively low ionization (i.e., with relatively strong [S II] emission relative to H $\alpha$ ) are skewed toward yellow or orange-brown, while higher ionization regions with strong [O III] show as blue or purplish (if H $\alpha$  is also present). Hence, one might see a bright H II region that varies from a blue or purple central region to having a yellowish-brown outer edge, indicating the ionization of the gas decreases as one moves further from the exciting stars. An isolated arcuate or shell-like structure that shows the yellowish-brown color is likely to be a shock-heated nebula such as a supernova remnant or perhaps a stellar wind-shocked region, where again the relative [S II] emission is strong (see Mathewson & Clarke 1973, Chen et al. 2000).

One cautionary note is that seeing an object in projection against a particular region of nebulosity is no guarantee that the object is associated with that nebulosity, especially for more diffuse regions of emission. Indeed, the position of a given object in front of, within, or behind the nebulosity in the context images cannot be judged from the context image alone. The exception is where an object is a member of a tight association or cluster that is clearly associated with a given nebular structure or shell (e.g., Danforth & Blair 2006). However, even in these

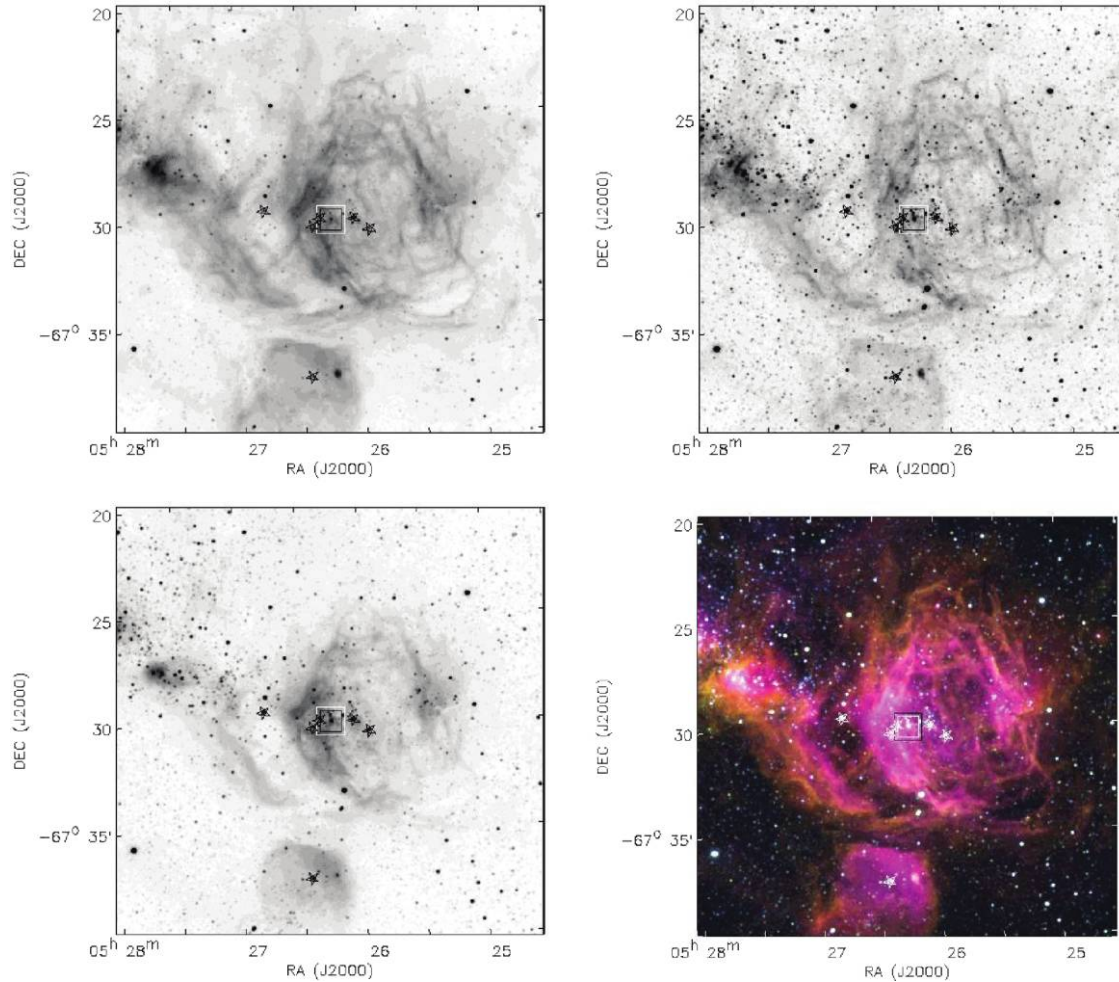


FIG. 6.—The MCELS  $H\alpha$  (upper left), [S II] (upper right), and [O III] (lower left) images (black and white), and a color composite of the three (see text), for the object A11101 SK-67°106. The *FUSE* target is centrally located and other objects observed with *FUSE* are indicated by star symbols.

cases, the star is centrally located while the emission likely surrounds the object, making it unclear what is in the foreground. In many cases it is the character of the absorption lines seen in the *FUSE* data in conjunction with the appearance of the context image that suggests an association (or not).

### 3.3.2. Infrared Context Images

The infrared context images are drawn from recent work with the *Spitzer Space Telescope*, and closely parallel the optical image display described above. As with the optical data, we select three bands to combine into a single color context image. We have chosen to show the IRAC 3.6  $\mu\text{m}$  (blue), IRAC 8  $\mu\text{m}$  (green) and MIPS 24  $\mu\text{m}$  data (red). The 3.6  $\mu\text{m}$  image is typically dominated by stars, but the 8  $\mu\text{m}$  band often shows significant nebular emission, primarily due to emission from polycyclic aromatic hydrocarbons (PAHs). Emission at 24  $\mu\text{m}$  is usually indicative of warm ISM dust. (Note: The spatial

resolution of the MIPS 24  $\mu\text{m}$  data is intrinsically lower than for the other images,  $\sim 6.2''$  compared with  $2''$  for IRAC.) In certain cases, a very localized red region surrounds a target star, indicating a dusty circumstellar shell (e.g., B09002, SK-67° 266, for one example).

For the SMC, we obtained the large mosaic images from the work of Bolatto et al. (2007), kindly made available by A. Bolatto. Using the World Coordinate System information in the FITS headers, the relevant subimages could be extracted directly in a manner similar to the optical data. The mosaic images provided coverage for  $\sim 85\%$  of the SMC sight lines in the infrared region.

The LMC *Spitzer* IRAC and MIPS context images were constructed mainly from the SAGE survey data (Meixner et al. 2006), using the Basic Calibrated Data (BCD) images produced by the standard *Spitzer* pipeline. For a complete list of the archival datasets used see Gruendl & Chu (2009). More information on the instruments and pipeline processing can be found at

the *Spitzer* Science Center's Observer Support website<sup>13</sup>. To combine the BCD images, we first solved for and removed brightness offsets between the individual frames using the method outlined by Regan & Gruendl (1995). The individual frames were then combined into mosaic images with a 20' FOV centered on each *FUSE* target using utilities in the MOPEX software package.

An example infrared field is shown in Figure 7, again with the individual data sets shown in black and white along with the assembled color composite. In general, the dynamic range in the *Spitzer* data is not as large as in the optical data, and this caused some differences in the way the data were combined into the color composite images. Although our program still looked at each subimage and set the background and display levels, a simple linear scaling worked better for displaying these data. Also, only two of the three IR bands selected tend to have nebular emission, so the range of color variations from overlapping regions is less than for the optical images. Regions showing both 8 and 24  $\mu\text{m}$  emission thus display as yellow (red plus green), as opposed to the more muted orange-brown for regions of red plus green in the optical display. Furthermore, since the number of visible stars drops off rapidly toward the longer wave bands, most of the stars are only present in the 3.6  $\mu\text{m}$  band, making them predominantly blue. While stars are sometimes visible in the box overlay indicating the *FUSE* sight line, in many cases the *FUSE* target itself does not show prominently in the IR context images. Note that the regions shown are exactly the same size as the optical FOVs, to simplify comparisons between the two sets of context images.

#### 4. OVERVIEW OF MAST HLSP SITE

We have made the materials described above available for each object in Tables 1 and 2, using an online interactive user interface at MAST, as part of the High Level Science Products (HLSP) program.<sup>14</sup> An overview of the functionality of this site and simple examples of its use follow.

##### 4.1. Overview Materials

The main page for the site contains introductory material, a README file describing the data processing and other general information, tips for navigating the site, and a link to overview images similar to Figures 1 and 2, both with and without the sight line indicators overlaid. Additional black and white images with coordinate overlays are provided to permit the 20' sight line images to be placed in an even broader spatial context. The main page also provides options for searching and selecting the data of interest. A request to search for a specific object brings up the normal MAST search page interface

<sup>13</sup>The online tables contain an additional column for the SIMBAD name that is not duplicated here.

<sup>14</sup> See [http://archive.stsci.edu/prepds/fuse\\_mc](http://archive.stsci.edu/prepds/fuse_mc).

available for many missions (including *FUSE*). However, the more powerful format for comparing and selecting data of interest is one of the options for obtaining a list of objects, either for the LMC, the SMC, or all objects in the MC atlas. This interface is described next.

##### 4.2. Search Results Table

The primary user interface is driven by a listing of information similar to Tables 1 and 2, which is called the "FUSE\_MC Search Results" table. We will refer to it as the interface table, because it provides access to the object-level supporting materials. The interface table contains two additional columns not shown in Table 1 or 2. At far left, a "Mark" column allows the user to indicate a data set for retrieval. When one or more data sets have been selected, the "Download marked data" button causes a Unix/Linux tar file to be created containing the *\*all\*.fits* and *\*nvo\*.fits* FITS format data files used for the atlas plots for the marked object(s). For those objects where multiple observations have been combined, this provides direct access to the combined data sets. Also, in addition to the *FUSE* Target Name, an alternate "SIMBAD Name" column is shown. This can be useful for finding individual objects, as the "Target Name" listed by a *FUSE* observer may be nonstandard. By default, the list is sorted on the *FUSE* Data ID field. It can be resorted on the various columns as desired (for instance, target name, spectral type, *V* magnitude, etc.) simply by selecting the column heading.

The interface table provides links to additional supporting information. As mentioned earlier, objects with multiple observations are indicated in the column "Num DS" (number of data sets), and the value in this column is linked to a list of the individual data sets that went into the combined data set. The entries for "Spectral Type Ref" and "Photometry Ref" are linked to the Bibliography entry that was used for the listed information. Links in the Bibliography listing provide direct access to the electronic versions of the references. For convenience, these references are also shown at the bottom of Tables 1 and 2 of this article.

##### 4.3. Object Summary Pages

By selecting a highlighted "Data ID" entry in the interface table, the user is redirected to a separate browser window where the *FUSE* Object Summary page is displayed, as shown in Figure 8. This is the page that contains the context images, *FUSE* ISM line summaries, and O VI and Spectral overview plots, as described. This separate window allows the user to retain access to the interface table even while displaying successive Target Summary pages. Hence, after inspection of a particular Object Summary page, a user could choose to mark a particular data set for retrieval or move on to display a new object summary.

The Object Summary pages provide additional links to information. In Figure 8, note the text block at top with basic sum-

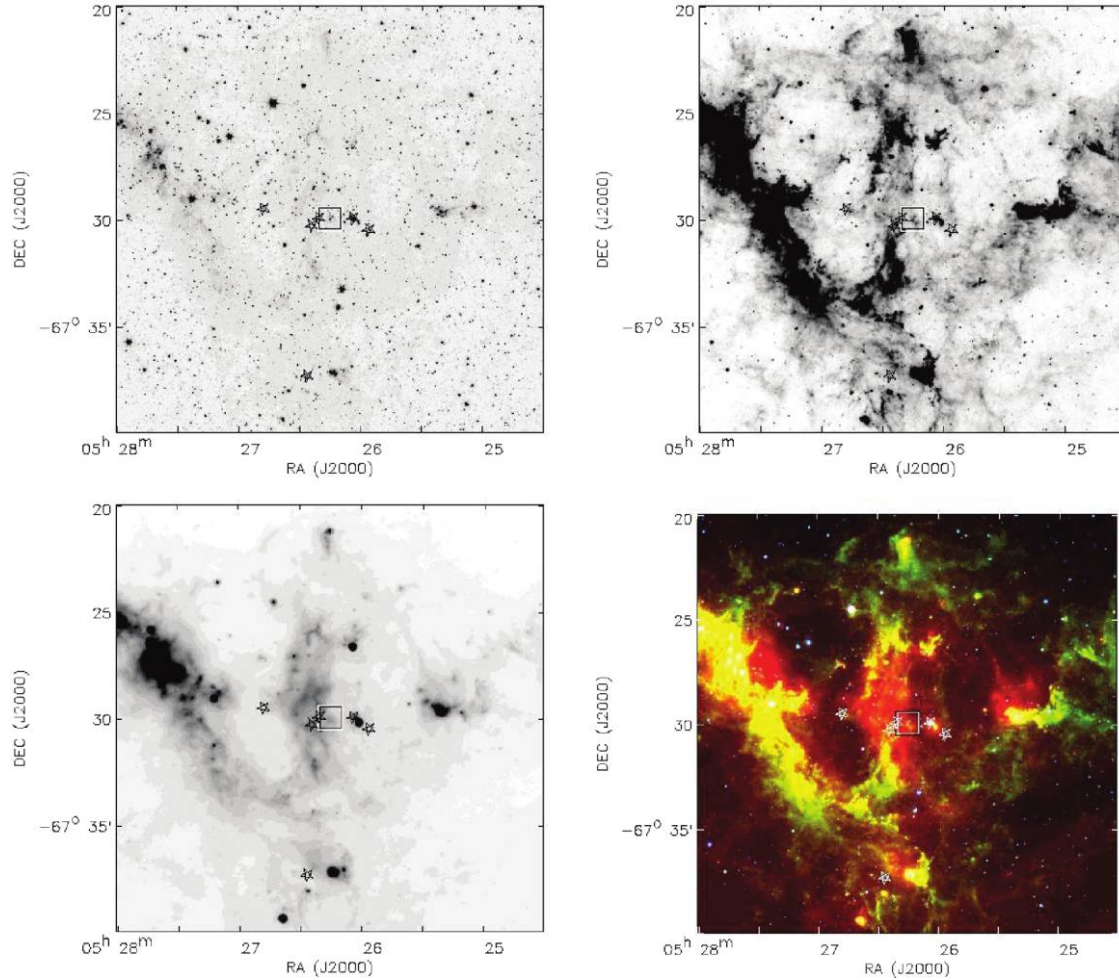


FIG. 7.—Infrared images for the same object as shown in Figure 6, A11101. The four panels show *Spitzer* 3.6  $\mu\text{m}$  (upper left), 8  $\mu\text{m}$  (upper right), and 24  $\mu\text{m}$  (lower left) frames (black and white), and a color composite of the three (see text).

mary information about the object. One of the entries is again the SIMBAD data base<sup>15</sup> identifier for the object. Selecting the highlighted SIMBAD name takes the user directly to the SIMBAD data base listing where additional information about the object is available. Selecting either of the color context images redirects the user to a page that shows the individual images that went into the color composite (in reverse black and white display), enlarged to show detail, and including a color composite view on the same scale for comparison (similar to the individual panels in Figures 5 and 6). The coordinate and other context information is duplicated on each individual frame for reference. Selecting any of the *FUSE* data plots on the Object Summary pages also links to a larger version of the plot, in case the user desires to see more detail than is visible on the

<sup>15</sup>These files are compatible for use in the National Virtual Observatory; see <http://www.us-vo.org>.

Summary page version. Any of the materials can be printed from within the user's browser interface.

#### 4.4. Examples

We now provide two simple examples that illustrate different aspects of how the materials might be used.

*Diagnosing a Particular Sight Line.* In the online materials, the reader is encouraged to load the Object Summary page for E51129, the star known as BI 130. The summary information at the top of the page indicates this is a  $V = 12.52$  O8.5  $V((f))$  star with modest reddening,  $E(B - V) = 0.14$ , observed by *FUSE* for some 11 ks in the LWRS aperture. The context images show the sight line is projected onto bright, low-ionization optical emission, which is accompanied by very substantial IR emission. Also, several other nearby stars have been observed with *FUSE*. Moving to the ISM line plots, one sees moderately strong ISM absorption at the Milky Way velocity ( $\sim 25 \text{ km s}^{-1}$ ), especially in the low ions and  $\text{H}_2$  lines. However, there is *no*

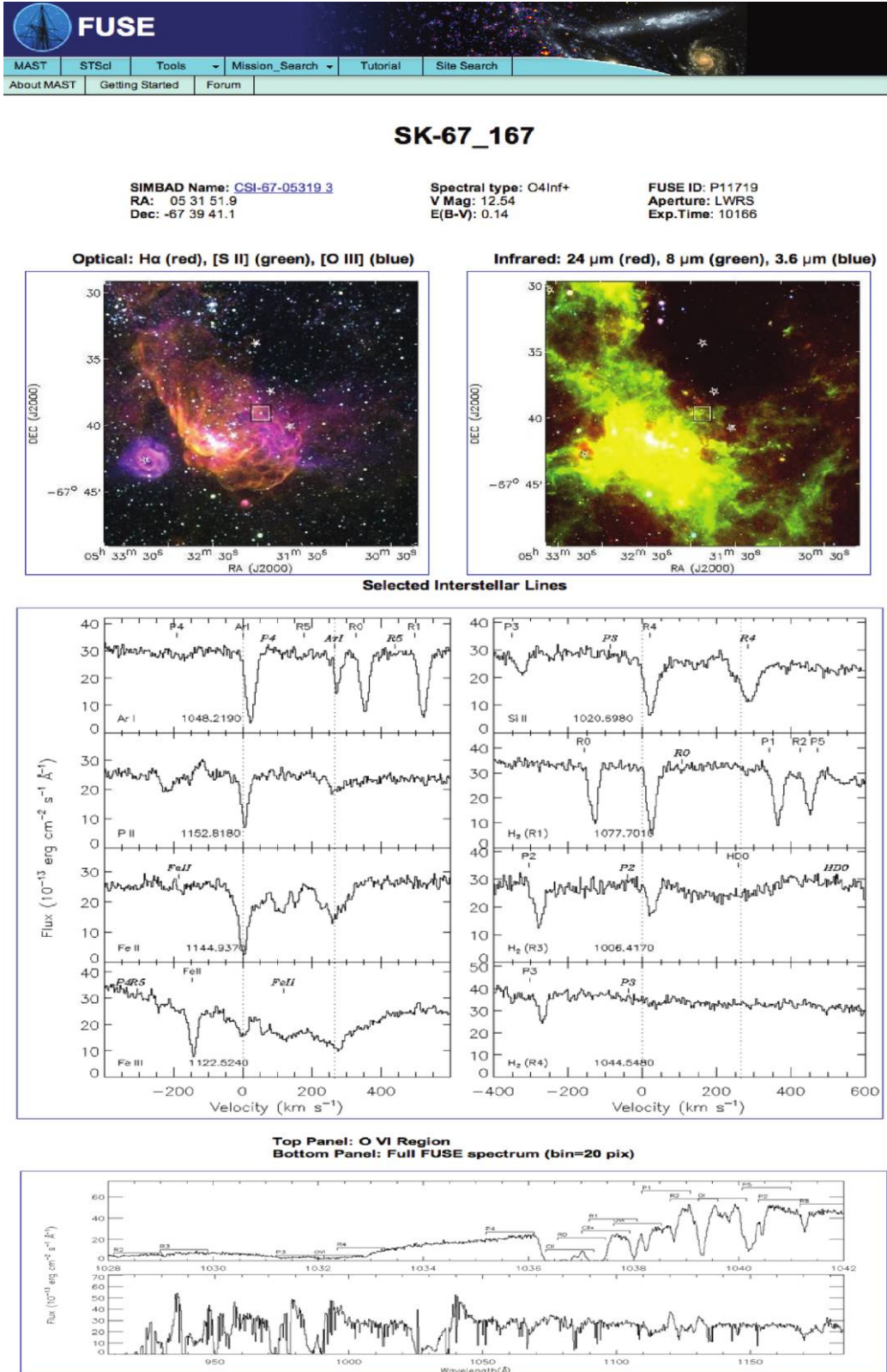


FIG. 8.—*FUSE* Target Summary page as it appears on the MAST HLSP site. The vertical scaling has been compressed, and only one of the two ISM panels is shown in this example.

*convincing evidence* of narrow LMC ISM line absorption at or near the nominal LMC velocity fiducial. The broad, complex absorption in the Fe II  $\lambda 1145$  panel centered near  $150 \text{ km s}^{-1}$  is not Fe II because no corresponding feature is seen in the Fe II  $\lambda 1125$  panel. The absorption in the S IV  $\lambda 1062$  panel at the LMC velocity is broad, and given the low-ionization nature of the potential absorbing material in the context images and no indication of higher ionization gas in the O VI  $\lambda 1032$  panel, this is unlikely to be ISM-related. The only potential hint of LMC ISM appears to be in the sensitive O I  $\lambda 1039$  line at just over  $200 \text{ km s}^{-1}$ . The conclusion that one reaches from this quick look is not only that the star must be in the foreground of the emission onto which it is projected, but that the star must be located on the near-side of the LMC in general, so that little LMC ISM of any kind is seen. Using the LMC image with coordinates that is displayed from the “Overview Images” page, one can see that this object is projected close to the center of the LMC (just north of the “Bar”). This is inconclusive, but at least consistent with a position on the front side of the LMC.

If one wanted to investigate this idea further, one could choose to look at some of the nearby *FUSE* sight lines for consistency. Going back to the LMC interface table, sort it on R.A. by selecting the top column header. This allows easy identification of the nearby *FUSE* targets seen in the context images by looking for stars near the same declination as the original object but at slightly higher right ascensions (because these stars are farther east in the context images).

*A Project-level Example.* Data from the International Ultraviolet Explorer (IUE) satellite (e.g., Savage & de Boer 1979, 1981; Wayte 1990) showed some sight lines toward the LMC with absorption at intermediate ( $\pm 70 \text{ km s}^{-1}$ ) and/or high velocities ( $+90$  to  $+140 \text{ km s}^{-1}$ ). This absorbing material probably arises from intermediate velocity clouds (IVCs) and high velocity clouds (HVCs) in the halo of our Galaxy (i.e., in the foreground of the LMC) that are patchy in their spatial distribution. The density of stellar sight lines covering the  $\sim 25$  square degrees of the LMC provides a unique opportunity to study the spatial distribution of these intervening clouds, and to characterize their metallicity and ionization structure. However, to do so one must first find the sight lines that show ISM spectral absorptions at the relevant IVC and/or HVC velocity ranges.

With an hour of dedicated effort one could make a preliminary pass through the LMC portion of the MC Legacy objects and empirically identify the data sets of most relevance. By

inspecting the context images, one might choose to eliminate (or at least flag separately) those sight lines projected against bright, structured nebosity (i.e., where blue-shifted LMC absorption from an expanding shell might cause intrinsic LMC absorption in the same velocity range as the IVC/HVC). One could also immediately link to the SIMBAD data base for these targets and identify which *FUSE* targets also had IUE data at longer wavelengths. A user might then want to mark and retrieve the *FUSE* data for key sight lines for quantitative measurement of ISM column densities and further analysis.

## 5. SUMMARY

The sensitivity of the *FUSE* satellite coupled with the typical brightness of the hottest stars in the Magellanic Clouds provided a powerful incentive to observers over the lifetime of the *FUSE* mission. Hundreds of observations, obtained either for studying the stars themselves or the ISM along each sight line, have provided a rich legacy to future researchers. Using the power of the ensemble data set requires that one have the means to assess the data to find the individual data sets that are appropriate to be used for a given scientific investigation. With the *FUSE*/MAST Magellanic Clouds Legacy web site, we have provided the tools to allow this rich data set to be efficiently accessed and mined by future researchers. It is our hope that this interface enables ongoing research into this rich resource by the community at large.

It is a pleasure to thank the *FUSE* operations team for their efforts in obtaining these data over eight years of science operations. We thank Sean Points, Chris Smith, Frank Winkler, and the entire MCELS team for providing us with the optical data used in this article. Alberto Bolotto and Snezana Stanimirovic provided *Spitzer* mosaics of their SMC data for our use, for which we are most grateful. We acknowledge Margaret Meixner and the *Spitzer* SAGE team for their dedication and foresight in crafting the SAGE survey of the LMC, and for making the data available to the community. Karen Levay and Randy Thompson of STScI/MAST have been instrumental in making these data sets available as a High Level Science Product to the astronomical community. This work has been supported by NASA grants NAG5-13704 and NNG05GE03G to the Johns Hopkins University.

## REFERENCES

- Ardeberg, A., Burnet, J. P., Maurice, E., & Prevot, L. 1972, *A&AS*, 6, 249  
 Ardeberg, A., & Maurice, E. 1977, *A&AS*, 30, 261  
 Azzopardi, M., & Vignneau, J. 1979, *A&AS*, 35, 353  
 Azzopardi, M., Vignneau, J., & Macquet, M. 1975, *A&AS*, 22, 285  
 Blair, W. P., Sankrit, R., Hoopes, C., et al. 2006, in ASP Conf. Ser. 348, *Astrophysics in the Far Ultraviolet: Five Years of Discovery with FUSE*, ed. G. Sonneborn, H. W. Moos, & B-G. Andersson, 127  
 Bolatto, A. D., et al. 2007, *ApJ*, 655, 212  
 Brunet, J. P., Imbert, N., Martin, N., Maines, P., Prevot, L., Rebeiro, E., & Rousseau, J. 1975, *A&AS*, 21, 109

- Chen, C-H. R., Chu, Y.Gruendl, R. A., & Points, S. D. 2000, AJ, 119, 1317
- Conti, P. S., Garmany, C. D., & Massey, P. 1986, AJ, 92, 48
- Crampton, D., & Greasley, J. 1982, PASP, 94, 31
- Crowther, P. A., De Marco, O., & Barlow, M. J. 1998, MNRAS, 296, 367
- Crowther, P. A., & Smith, L. J. 1997, A&A, 320, 500
- Danforth, C. W., Howk, J. C., Fullerton, A. W., Blair, W. P., & Sembach, K. R. 2002, ApJS, 139, 81
- Dixon, W. V., et al. 2007, PASP, 119, 527
- Feitzinger, J. V., & Isserstedt, J. 1983, A&AS, 51, 505
- Fitzpatrick, E. L. 1988, ApJ, 335, 703
- . 1991, PASP, 103, 1123
- Garmany, C. D., Conti, P. S., & Massey, P. 1987, AJ, 93, 1070
- Garmany, C. D., & Walborn, N. R. 1987, PASP, 99, 240
- Gruendl, R. A., & Chu, Y.-H. 2009, ApJS, submitted
- Heydari-Malayeri, M., & Hutsemekers, D. 1991, A&A, 244, 64
- Howk, J. C., Savage, B. D., Sembach, K. R., & Hoopes, C. G. 2002b, ApJ, 572, 264
- Hoopes, C. G., Sembach, K. R., Howk, J. C., Savage, B. D., & Fullerton, A. W. 2002, ApJ, 569, 233
- Howk, J. C., Sembach, K. R., Roth, K. C., & Kruk, J. W. 2000, ApJ, 544, 867
- Howk, J. C., Sembach, K. R., Savage, B. D., Massa, D., Friedman, S. D., & Fullerton, A. W. 2002a, ApJ, 569, 214
- Hutchings, J. B., & Giasson, J. 2001, PASP, 113, 1205
- Isserstedt, J. 1975, A&AS, 19, 259
- . 1978, A&AS, 33, 193
- . 1982, A&AS, 50, 7
- Jaxon, E. G., Guerro, M. A., Howk, J. C., Walborn, N. R., Chu, Y.-H., & Wakker, B. P. 2001, PASP, 113, 1130
- Koenigsberger, G., Moffat, A. F. J., St. Louis, N., Auer, L. H., Drissen, L., & Seggewiss, W. 1994, ApJ, 436, 301
- Lennon, D. J. 1997, A&A, 317, 871
- Lupton, R., Blanton, M. R., Fekete, G., Hogg, D. W., O'Mullane, W., Szalay, A., & Wherry, N. 2004, PASP, 116, 133
- Massa, D., Fullerton, A., Hutchings, J., et al. 2000, ApJ, 538, L47
- Massa, D., et al. 2003, ApJ, 586, 996
- Massey, P. 2002, ApJS, 141, 81
- Massey, P., & Duffy, A. S. 2001, ApJ, 550, 713
- Massey, P., & Hunter, D. A. 1998, ApJ, 493, 180
- Massey, P., Lang, C. C., Degioia-Eastwood, K., & Garmany, C. D. 1995, ApJ, 438, 188
- Massey, P., Parker, J. W., & Garmany, C. D. 1989, AJ, 98, 1305
- Mathewson, D. S., & Clarke, J. N. 1973, ApJ, 180, 725
- Meixner, M., et al. 2006, AJ, 132, 2268
- Moffat, A. F. J., Niemela, V. S., & Marraco, H. G. 1990, ApJ, 348, 232
- Moos, H. W., Cash, W., Cowie, L., et al. 2000, ApJ, 538, L1
- Moos, H. W., et al. 2002, ApJS, 140, 3
- Morton, D. C. 2003, ApJS, 149, 205
- Morton, D. C., & Dinerstein, H. L. 1976, ApJ, 204, 1
- Regan, M. W., & Gruendl, R. A. 1995, in ASP Conf. Ser. 77, ADASS IV Proceedings, ed. R. A. Shaw, H. E. Payne, & J. J. E. Hayes, 335
- Rousseau, J., Martin, N., Prevot, L., Rebeiro, E., Robin, A., & Brunet, J. P. 1978, A&AS, 31, 243
- Sahnow, D. J., et al. 2000, ApJ, 538, L7
- Savage, B. D., & de Boer, K. S. 1979, ApJ, 230, L77
- . 1981, ApJ, 243, 460
- Sembach, K. R., Howk, J. C., Savage, B. D., & Shull, J. M. 2001, AJ, 121, 992
- Smith, R. C., The MCELS Team 1999, IAU Symp. 190, New Views of the Magellanic Clouds, ed. Y.-H. Chu, N. Suntzeff, J. Hesser, & D. Bohlender, 28
- Smith, R. C., Points, S., Aguilera, C., Leiton, R., Chu, Y.-H., & Winkler, P. F. 2004, BAAS, 205, 1511, #101.08
- Smith, R. C., Points, S., Aguilera, C., Leiton, R., Chu, Y.-H., Winkler, P. F., Aguilera, C., & Leiton, R. 2005, BAAS, 207, 1200, #25.07
- Smith, L. F., Shara, M. M., & Moffat, A. F. J. 1996, MNRAS, 281, 163
- Spitzer, L. 1978, Physical Processes in the Interstellar Medium, (New York: Wiley-Interscience)
- Torres-Dodgen, A. V., & Massey, P. 1988, AJ, 96, 1076
- Tumlinson, J., et al. 2002, ApJ, 566, 857
- Walborn, N. R. 1977, ApJ, 215, 53
- . 1982, ApJ, 254, L15
- . 1983, ApJ, 265, 716
- Walborn, N. R., & Blades, J. C. 1986, ApJ, 304, L17
- . 1997, ApJS, 112, 457
- Walborn, N. R., Lennon, D. J., Haser, S. M., Kudritzki, R.-P., & Voels, S. A. 1995, PASP, 107, 104
- Walborn, N. R., Lennon, D. J., Heap, S. R., Lindler, D. J., Smith, L. J., Evans, C. J., & Parker, J. W. 2000, PASP, 112, 1243
- Walborn, N. R., et al. 2002a, AJ, 123, 2754
- Walborn, N. R., et al. 2002b, ApJS, 141, 443
- Wayte, S. R. 1990, ApJ, 355, 473
- Willis, A. J., Crowther, P. A., Fullerton, A. J. et al., 2004, ApJS, 154, 651
- Winkler, P. F., Young, A., Braziunas, D., et al. 2005, BAAS, 207, 1380, #132.03
- Zaritsky, D., Harris, J., Thompson, I. B., Grebel, E. K., & Massey, P. 2002, AJ, 123, 855